

# Study on redeposition of eroded finer particles during suffusion with image processing

Kuang Cheng<sup>a,b</sup>, Hang Lu<sup>a</sup>, Xiangkun Cui<sup>a</sup>, Jiacheng Ma<sup>a</sup>, and Ha H. Bui<sup>b</sup>

<sup>a</sup>College of Civil Engineering and Architecture, Hebei University, Baoding 071002, China; <sup>b</sup>Department of Civil and Environmental Engineering, Monash University, Australia

Corresponding author: Ha H. Bui (email: [ha.bui@monash.edu](mailto:ha.bui@monash.edu))

## Abstract

An image processing-based approach is developed and integrated into the one-dimensional suffusion tests to quantify the redeposition of eroded finer particles along the seepage direction. The results indicate that the redeposition mass of eroded finer particles exhibits an exponential decay along the seepage direction across various soil gradations and hydraulic conditions. A theoretical relationship is established between this exponential decay and the redeposition probability. Furthermore, the redeposition probability is found to be negatively related to the content of finer fraction, which is demonstrated to be rooted in the transition from a homogeneous to a localized distribution of redeposition position within the cross-section as the content of finer fraction increases from 15% to 35%.

**Key words:** erosion, earth dams, seepage, suffusion, redeposition

## Résumé

Une approche basée sur le traitement d'images a été développée et intégrée aux essais de suffusion unidimensionnels afin de quantifier la redéposition des particules fines érodées dans la direction de l'écoulement. Les résultats indiquent que la masse redéposée des particules fines érodées présente une décroissance exponentielle dans la direction de l'écoulement, et ce, pour différentes granulométries de sol et conditions hydrauliques. Une relation théorique a été établie entre cette décroissance exponentielle et la probabilité de redéposition. De plus, la probabilité de redéposition s'est révélée négativement corrélée à la teneur en fraction fine, ce qui s'explique par la transition d'une distribution homogène à une distribution localisée de la position de redéposition dans la section transversale, à mesure que la teneur en fraction fine augmente de 15 % à 35 %.

**Mots-clés :** érosion, barrages en terre, écoulement, suffusion, redéposition

## 1. Introduction

Suffusion involves the migration of finer particles within the voids of coarse skeletons in soils under seepage flow (Wan and Fell 2008). It is often encountered in soils featured by relatively wide particle size distributions (PSDs) without sufficient medium-sized particles, e.g., gap-graded soils featured by a hiatus of particle sizes and concave upward soils with PSDs having a flat fine tail and a steep coarser fraction (Chang and Zhang 2013). During suffusion, the finer particles are transported by the seepage flow within the voids of the coarse skeleton, and some of them are washed out from the soil matrix. The finer particle loss has gained special attention in previous research (Indraratna et al. 2018; Annapareddy et al. 2024; Cheng et al. 2024a, 2024b) since it is a fundamental mechanism for the development of suffusion and the associated seepage failure of earth structures, e.g., dam foundations (Luo et al. 2017), colluvial slopes (Cui et al. 2017), and soil-rock mixture embankments (Johnston et al. 2021, 2023). Apart from the loss of finer particles, some

finer particles washed out (or eroded) from the upstream soils may be redeposited within the downstream soils during their transportation by seepage flow (Sibille et al. 2015; Marot et al. 2016; Yang et al. 2019; Choe et al. 2024). The redeposition of eroded finer particles is also critical for the failure of real-life dam foundations and slopes. For example, Luo et al. (2017) demonstrate that the finer particles eroded from the upstream side of a cutoff wall in the dam foundations may be redeposited within the downstream side of the cutoff wall. It leads to an increased pore water pressure and decreased effective stress around the redeposition position, which further affects the deformation of dam foundations during the development of suffusion (Horikoshi and Takahashi 2015; Luo et al. 2017). Besides, the redeposition of eroded finer particles has been found to occur within the slope toe and the lower layer of the slope, which may lead to an increase in the local pore water pressure and a generation of weak layers that play a critical role in the failure of colluvial slopes under rainfall (Cui et al. 2017; Johnston et al. 2023). Actually, the

redeposition of eroded finer particles affects the distribution of finer particles within the soils and thereby influences the evolution of hydro-mechanical properties of soils during suffusion. Therefore, it is crucial to have a better understanding of the redeposition of eroded finer particles during suffusion.

Several research works (Chang and Zhang 2011; Ke and Takahashi 2014; Benamar et al. 2019) investigate the distribution of finer particles within 1D soil columns after suffusion tests. In these studies, the soil columns are removed in several layers after suffusion tests, and their PSDs are obtained by sieving to evaluate the loss of finer particles in each layer. Kenney and Lau (1985) divide the soil columns into six layers for sieving. They found that the contents of finer particles within the downstream soil columns are generally larger than those in the upstream soil columns. Similar observations are also obtained by subsequent research in various situations, e.g., upward (Benamar et al. 2019) or downward (Mehdizadeh et al. 2021; Prasomsri and Takahashi 2021) seepage flow, multiple seepages (Prasomsri and Takahashi 2021), step-wised or constant hydraulic gradient (Rochim et al. 2017), samples under gravity with no surcharging (Rochim et al. 2017; Benamar et al. 2019), samples under one-dimensional consolidation (Kenney and Lau 1985), triaxial isotropic (Prasomsri and Takahashi 2021) or anisotropic (Chang and Zhang 2011) compression. A higher content of finer particles in the downstream soil column should be due to the downstream redeposition of the eroded finer particles washed out from the upstream soil column during suffusion, as demonstrated by Ke and Takahashi (2012) and Mehdizadeh et al. (2021). The sieving analysis results after suffusion generally support the hypothesis of the redeposition of the eroded finer particles during suffusion, although a direct observation of the redeposition is not possible by only using sieving analysis.

For direct observation of the evolution of the distribution of finer particles within the voids of the coarse skeleton during suffusion, several visualization techniques have been introduced, such as plane laser-induced fluorescence (Hunter and Brown 2018; Deng and Wang 2022) and X-ray-computed tomography (Nguyen et al. 2019; Xia et al. 2024). Besides, the coupled modelling of suffusion using the computational fluid dynamics and the discrete element method provides further insight into the redeposition of eroded finer particles and the associated fabric evolution during suffusion (Cheng et al. 2018; Mu et al. 2023). The observations from these techniques confirm the redeposition of eroded finer particles during suffusion and shed light on the micro-scale or pore-scale mechanisms of redeposition during suffusion. However, a quantitative evaluation of redeposition within each layer of the downstream soil column is still needed. It is unknown how the soil gradations (e.g., content of finer fraction, gap ratio) and the hydraulic conditions will affect redeposition. Although several research (Lei et al. 2017; Yang et al. 2019; Ma et al. 2022) implement redeposition law into the continuum model for suffusion, the quantitative description of redeposition is based on a hypothesis that still lack experimental validations.

This study is mainly focused on quantifying the redeposition of eroded finer particles within the downstream soil matrix during suffusion. For this purpose, an image processing-

based approach is developed and incorporated into the one-dimensional suffusion tests to quantify redeposition along the seepage direction. A typical exponential decay for the redeposition of eroded finer particles along the seepage direction is observed for various soil gradations and hydraulic conditions. Meanwhile, theoretical analyses are performed to gain insight into the exponential decay of redeposition from the perspective of redeposition probability. Finally, the redeposition probability is found to be negatively correlated to the content of the finer fraction, which is further explained from the perspective of redeposition pattern.

## 2. Materials and methods

### 2.1. Testing materials

Typical gap-graded soils with various contents of finer fraction,  $F_c$ , and different size ratios,  $D_{15}'/d_{85}'$ , are considered in the experimental tests, as shown in Fig. 1 and Table 1, in which  $D_{15}'$  is the diameter corresponding to 15% passing of coarser fraction's PSD, while  $d_{85}'$  is the diameter corresponding to 85% passing of finer fraction's PSD. It is noteworthy that the "finer fraction" refers to the particles with relatively smaller sizes compared to the coarser particles in gap-graded soils, as shown in Fig. 1. It is different from the definition of "fine particles" or "fines" with diameters smaller than 0.075 mm (or 0.063 mm) in geotechnical standards (e.g., ASTM D2487-11 (2011)). Although fines may have important influence on the internal stability of soils as demonstrated by Wan and Fell (2008) and Chang and Zhang (2013), they are not considered herein for simplicity. The gap-graded soils tested are evaluated to be very susceptible to suffusion according to two typical internal stability criteria, i.e., Chang and Zhang (2013) criterion and CSD (Constriction Size Distribution)-based criterion (Indraratna et al. 2015, 2022), as presented in Table S1 of Supplementary Information. The minimum and maximum void ratios of soils are determined using the procedures proposed by Lade et al. (1998), as listed in Table 1. The details of the procedures are described in Section S2 of the Supplementary Information. The soils consist of silica sands\gravels, the images of which are presented in Fig. 1. The properties of the silica sands\gravels are detailed in Table S2 of the Supplementary Information. Note that both white and red silica sands are used as the finer fraction to facilitate the quantification of the redeposition of eroded finer particles, which will be detailed in Section 3. The roundness of the sand\gravel grains is calculated with the method given by Kuo and Freeman (2000), in the high-resolution images of the grains are taken for the calculation of roundness using MATLAB. The results show that the finer white and red particles have similar shapes (see Table S2 of the Supplementary Information).

### 2.2. Experimental setup

The suffusion tests are conducted using a customized equipment, as illustrated in Fig. 2. A comprehensive description of the equipment is provided in Section S3 of the Supplementary Information. In particular, the soil column is 210 mm in height (note that it is increased to 270 mm for

**Fig. 1.** Particle size distributions of tested gap-graded soils with various contents of finer fraction,  $F_c$ , and different size ratios of coarser to finer fractions,  $D_{15}'/d_{85}'$ .

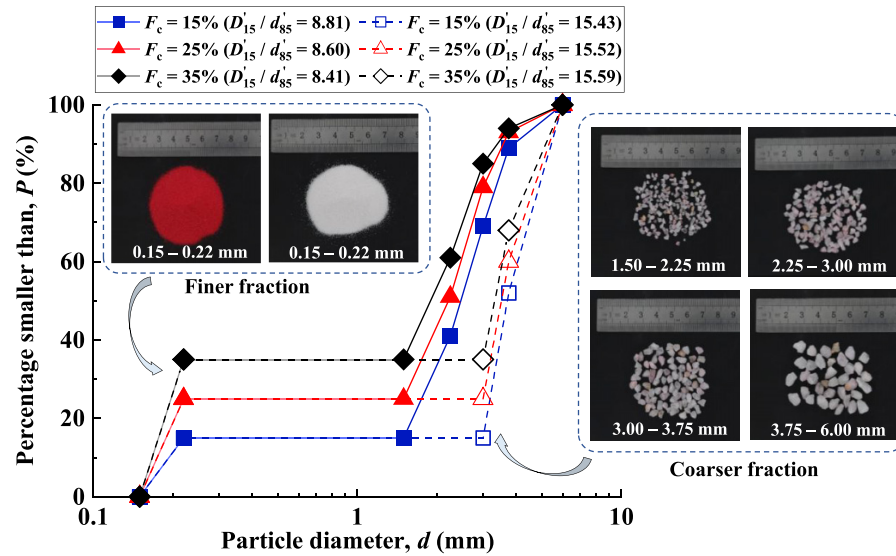


**Table 1.** List of index properties of gap-graded soils.

Symbol	Maximum void ratio, $e_{\max}$	Minimum void ratio, $e_{\min}$	Content of finer fraction, $F_c$ (%)	$D_{15}'/d_{85}'$
FC15-GN	0.899	0.416	15	8.81
FC25-GN	0.842	0.342	25	8.60
FC35-GN	0.726	0.309	35	8.41
FC15-GW	0.861	0.413	15	15.43
FC25-GW	0.620	0.305	25	15.52
FC35-GW	0.591	0.281	35	15.59

**Fig. 2.** Schematic for the suffusion testing equipment.

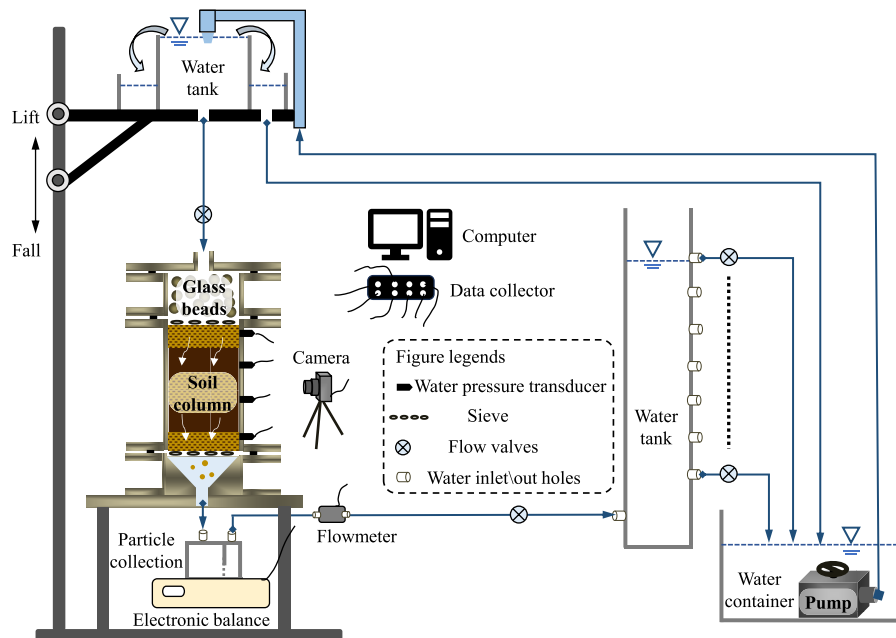
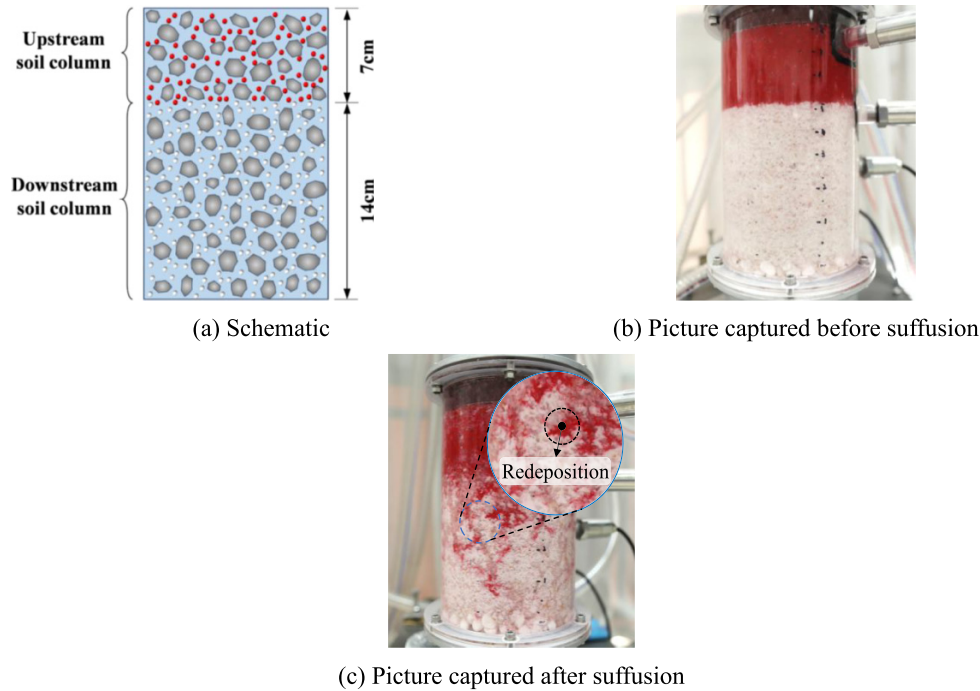


**Fig. 3.** The upstream and downstream soil columns, with finer red and white particles packed in voids of the coarse skeleton, respectively.



certain samples to accommodate an additional overlying soil and 150 mm in diameter. The column diameter is selected to be 25 times the maximum particle size, which is sufficient to mitigate preferential flow along the side wall (Moffat et al. 2011). Constant hydraulic gradients, up to a maximum of 10, could be applied to the soil column using the upstream and downstream water tanks with adjustable water levels (see Fig. 2). A particle collection system is employed to isolate and measure the mass of eroded finer particle from the outlet water flow. Water flowrates and hydraulic gradients within the soil samples are monitored using a flowmeter (IHGYG-A10-DRS: 3–20 L/min,  $\pm 1.0\%$ ; GF-04: 0.08–4.17 L/min,  $\pm 1.0\%$ ; note that two flowmeters with different measurement ranges are used for samples with relatively high and low hydraulic conductivities, respectively) and pore water pressure transducers (0–35 kPa,  $\pm 0.3\%$ ; BP9325), respectively.

### 2.3. Soil column preparation

The gap-graded soils are prepared using a moist tamping method (Ke and Takahashi 2012) to prevent separation of the coarser and finer fractions. In this approach, the coarser and finer particles are pre-mixed with an initial water content of 3%. Then, they are carefully deposited into the soil column in 10 layers. For each layer, the soil is compacted to the specified density using a rubber hammer. The packing densities of all samples are controlled to be medium dense, corresponding to a relative density of approximately 53%. Saturation of the sample is performed by purging de-aired water into the sample from the bottom at a very slow rate for 2–3 h. To examine the repeatability and uniformity of the prepared samples, preliminary tests are conducted and additional three samples

( $F_c = 25\%$ , target void ratio is 0.577) are prepared using a similar technique. The overall void ratio is measured for each sample. Meanwhile, for each sample, it is sampled in five layers and the void ratio and finer fraction of each layer are measured. The overall void ratios for the three samples are found similar (the maximum deviation is no more than 0.005). For each sample, there are certain fluctuations among each layer for the void ratio and the finer fraction, while the maximum deviation is less than 0.005 for void ratio and 0.3% for finer fraction. These results confirm the repeatability and uniformity of the prepared samples.

Finer particles colored red (see Fig. 1) are used to pack the top third of the soil column (7 cm in height), while finer white particles (see Fig. 1) are used for the bottom two-thirds of the soil column (14 cm in height), as shown in Fig. 3. This specific arrangement is implemented to facilitate quantification of the downstream redeposition of finer particles eroded from the upstream soil skeleton using an image processing technique, which is described in detail in Section 3. Hereafter, the top third of the soil column, packed with finer red particles, will be referred to as the “upstream soil column”, while the bottom two-thirds, packed with finer white particles, will be referred to as the “downstream soil column”.

### 2.4. Experimental scenarios and conditions

A wide range of scenarios are considered, including various combinations of upstream and downstream soil columns with different contents of finer fraction (i.e.,  $F_c^{\text{up}} = 15\%, 25\%$ , and  $35\%$ ;  $F_c^{\text{down}} = 0\%, 15\%, 25\%$ , and  $35\%$ ), different methods for applying hydraulic gradients (i.e., step-wised or constant; see Fig. 4), varying water flowrates, and the presence of addi-



Fig. 4. Schematic of different manners for applying the hydraulic gradient,  $i$ .

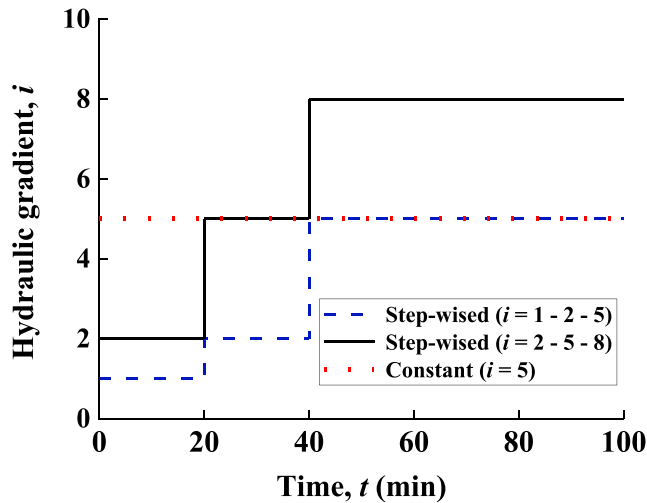
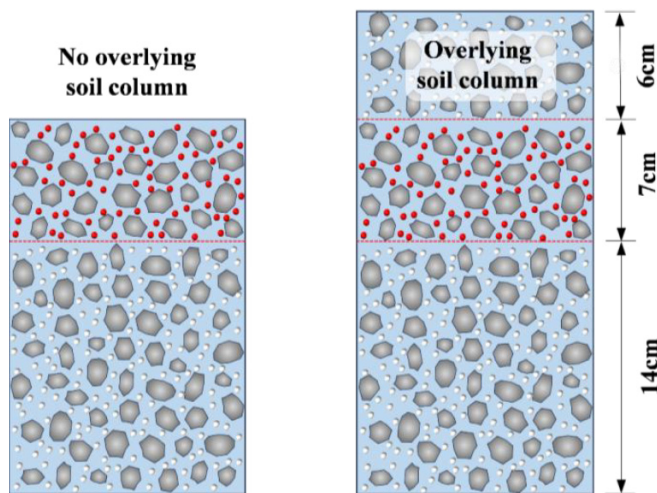


Fig. 5. Schematic for overlying soil layer above the upstream soil column.



tional overlying soil layers on the upstream soil column (see Fig. 5). Note that in the cases with overlying soil layers, the downstream redeposition of the finer particles in red washed out from the upstream soil column is quantified, similar to other cases. Details of the experimental conditions are provided in Section S4 and summarized in Table S3 of the Supplementary Information.

### 3. Quantification of redeposition of eroded finer particles: an image processing-based approach

As previously mentioned, the finer red particles in the upstream soil column are eroded by the downward seepage flow and then partially deposited in the downstream soil skeleton with finer white particles packed in the voids during suffu-

sion tests (see Fig. 3). As a result, the finer red particles are mixed with the white ones in the downstream soil column after suffusion, as shown in Fig. 3c. However, quantifying the mass of the finer red particles in the mixture of finer red and white particles using only a sieving method is challenging due to the similar sizes of the finer red and white particles. To address this, an image processing-based approach is proposed to measure the mass of finer red particles within the mixture.

#### 3.1. Proportion of finer red particles within the mixture: correlation establishment

Generally, the finer red and white particles should contribute differently to the grey value of an image capturing their mixture. Thus, it is reasonable to infer that the proportion of finer red particles in the mixture correlates with the grey value of the image.

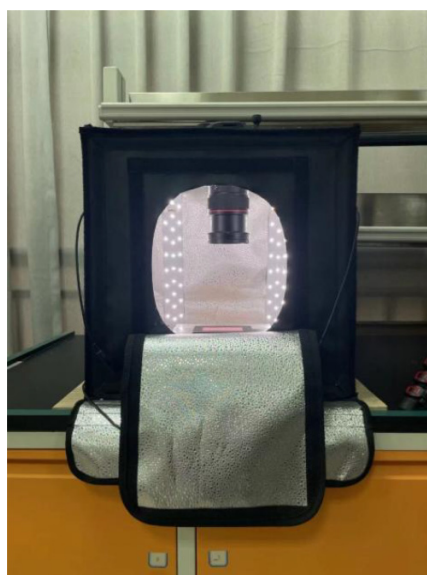
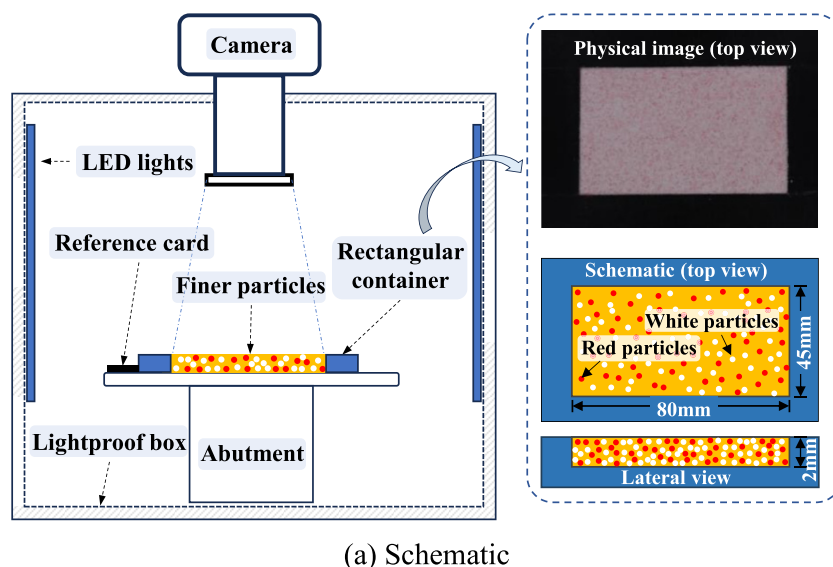
A custom lightproof box, as illustrated in Fig. 6, is designed to capture images of mixtures of finer red and white particles. This setup helps establish the correlation between the proportion of finer red particles in the mixture and the mean grey value of the image.

Mixtures of finer red and white particles with varying proportions of finer red particles,  $\alpha_{\text{red}}$ , ranging from 0% to 30% are prepared. These mixtures are deposited into a rectangular container measuring 80 mm in length, 45 mm in width, and 2 mm in height for the capturing of images, as illustrated in Fig. 6a. Note that the 2 mm height is selected to be around 10 times the maximum diameter of the finer particles, allowing for the creation of several layers of particles within the container. Then, the rectangular container is placed inside the lightproof box equipped with LED lights (Fig. 6) to prevent interference from external light sources that could affect the grey values of the images. A high-resolution camera (6260 × 4185 pixels; Canon EOS 6D Mark II) is placed on the top of the box to capture the images of the top view of the rectangular container filled with mixtures of finer red and white particles. The distance between the camera and the surface of the rectangular container is 18 cm. A black card is positioned next to the container to serve as a reference for monitoring potential fluctuations in LED light intensity. The relative variation in the grey values of the black card across all tests is found to be no more than 5% (see Fig. 7), confirming that the light intensity fluctuations are negligible.

The image resolution is 2850 × 1603 pixels for the 80 mm × 45 mm rectangular container, resulting in a pixel size of approximately 0.028 mm. Given that the smallest finer particles have a diameter of 0.15 mm, each particle occupies at least 28 pixel blocks. Preliminary tests indicate that this resolution is sufficient for the study's needs, as the focus is the mean grey value of the images rather than precise particle recognitions.

Based on the above experimental technique, the grey values of the mixtures packed in the rectangle container (see Fig. 6) of the lightproof box are obtained for mixtures with various proportions of finer red particles. It is noteworthy that the red particles may lose their color due to flow-induced rinsing effect, and at the same time the white particles may

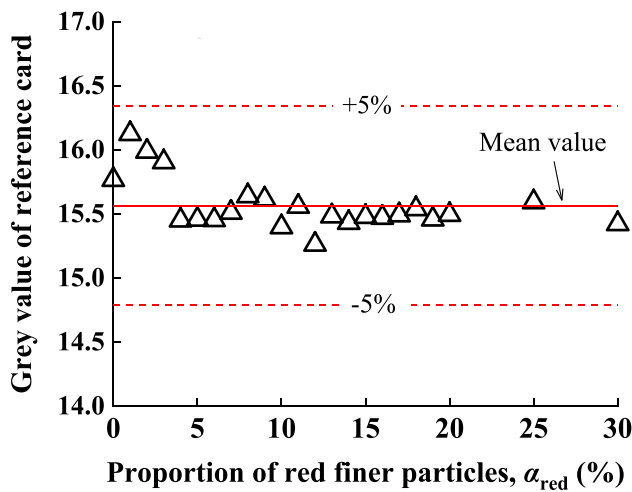
**Fig. 6.** The customized lightproof box for capturing images of mixtures of finer red and white particles (the distance between the camera and the surface of the rectangle container is 18 cm).



become dyed red by the water flow from the upstream layer formed of red particles (although the color change is barely perceptible to the naked eye) in the suffusion tests. To mimic the possible color changes of red and white particles during suffusion tests, additional seepage tests are conducted on soil columns packed with layered red and white particles, as illustrated in Fig. 8. The red and white particles used in the seepage tests are the same as those finer particles used in the suffusion tests. The duration of the seepage tests is 100 min, which is consistent to that of the suffusion tests. After the seepage tests, the red and white particles are sampled, respectively, and then used to test the grey values of their mixtures with different proportions of red particles. Note that the red and white particles may suffer from flow-induced rinsing and dying effect, respectively, during the seepage tests,

which is similar to that in the suffusion tests. On the other hand, the red and white particles not suffering from flow-induced rinsing and dying effect are also used to test the grey values of their mixtures for comparison. The correlations between the grey value of the mixture and the proportion of red particles in the mixture are obtained as shown in Fig. 8. The mean grey value,  $GR_m$ , of the mixture has a bilinear correlation to the proportion of red particles for both samples with and without suffering from flow-induced rinsing and dying effect. Meanwhile, the  $GR_m$  of the mixtures suffering from rinsing and dying effect is slightly smaller than that not suffering from rinsing and dying effect. This is because the dying of white particles leads to a decrease in the grey value of the white particles, and thereby a smaller  $GR_m$  at the same proportion of red particles. Nevertheless,

**Fig. 7.** Examination on the light fluctuation within the light-proof box using a reference card in black (in which different  $\alpha_{\text{red}}$  indicates different tests for capturing the pictures of mixtures of finer red and white particles; the vertical axis represents the mean grey value of the reference card).



the relatively error is no more than 3.5%. To consider the effect of flow-induced particle color change, the correlation obtained for the samples suffering from flow-induced rinsing and dying effect is subsequently used to quantify the downstream redeposition of the eroded finer particles, specifically the proportion of the finer red particles within the mixture of finer red and white particles in the downstream soil column.

### 3.2. Quantification of redeposition of eroded finer particles

The redeposition of the finer particles eroded from the upstream soil column varies along the seepage direction (see Fig. 3c), which is a key focus of this study. To analyze this variation, the downstream soil column (i.e., the bottom two-thirds of the soil column) is taken out layer by layer in seven layers, with a thickness of 2 cm for each layer, after the suffusion tests, as illustrated in Fig. 9a.

The particles from these layers are dried and sieved to separate finer particles from coarser ones (see Fig. 9b). The sieved finer particles, a mixture of red and white particles, are mixed uniformly for each layer. The mixture are then placed in the rectangular container (see Fig. 6), and images of the mixtures from each layer are captured in the light-proof box (see Fig. 9c). The mean grey value of each image is obtained (see Fig. 9d), which is used to determine the proportion of finer red particles in the mixture from each layer using the correlation shown in Fig. 8 (see Fig. 9e). Given that the total mass of finer particles in each layer is measured by sieving after the suffusion tests, the mass of finer red particles deposited in each layer could be calculated once the proportion of finer red particles in the mixture is obtained. These data will be used to quantify the downward redeposition of the finer particles eroded from the up-

stream soil column, which will be detailed in the following sections.

## 4. Variation of redeposition ratio of eroded finer particles along seepage direction

### 4.1. Redeposition ratio per seepage length, $\gamma_d$ : definition, calculation, and validation

To quantify the redeposition of eroded finer particles in the downstream soil skeleton, a redeposition ratio per seepage length, denoted as  $\gamma_d$ , is defined as follows:

$$(1) \quad \gamma_{di} = \frac{m_{di}/M_e}{\Delta z_i/D_{\max}} \times 100\%$$

where  $M_e$  is the total mass of the finer red particles washed out of the upstream soil column (i.e., the column consisting of finer red particles as illustrated in Fig. 3);  $m_{di}$  is the mass of the finer red particles washed out from the upstream soil column and subsequently deposited within the  $i$ th sublayer of the downstream soil column, as illustrated in Fig. 10; and  $\Delta z_i/D_{\max}$  represents the normalized thickness of each sublayer by the maximum diameter,  $D_{\max}$ , of coarser particles. It is noted that only a portion of the eroded or fluidized finer particles from the upstream soil column is washed out through its bottom; some of the eroded finer particles may be redeposited within the upstream soil column itself, a process referred to as “self-redeposition” (or “self-clogging”). This study focuses primarily on the redeposition of the finer particles in the downstream column that have been washed out from the upstream column while does not consider the self-redeposition of eroded finer particles within the upstream soil column.

For the experiments, the downstream soil column is uniformly divided into seven sublayers (see Fig. 9a) to calculate  $m_{di}$  and  $\gamma_{di}$ . The thickness,  $\Delta z_i$ , of each sublayer is set at 20 mm, which is approximately three to four times the maximum diameter of coarser particles. It is noteworthy that a pore body is generally considered as the pore space within a tetrahedron formed of four particles (Shire and O’Sullivan 2016). Therefore, three layers of particles are generally able to accommodate an entire pore body—constriction system, as illustrated in Fig. 10. Thus, the sublayers with thickness of around three to four times the maximum diameter of coarser particles are expected to accommodate at least one pore body—constriction system, which could be considered as one complete fundamental unit for the redeposition of finer particles. Note that only the top six sublayers are considered in the analyses, as the seventh sublayer is adjacent to the filter layer beneath the soil column (see Fig. 3) and may be affected by boundary effects.

In the experimental tests, the total mass,  $M_e$ , of eroded finer particles washed out from the upstream soil column (see Fig. 10) is calculated as the difference between the mass of the finer particles before and after suffusion in the upstream soil column, which could be easily determined using sieving analyses. The mass of finer particles ( $m_{di}$ ) washed out

**Fig. 8.** Correlations between mean grey value,  $GR_m$ , of the finer red and white particle mixtures with the proportion of finer red particles,  $\alpha_{red}$ , within the mixture (“rinsing and dying” represents that the red and white particles used to form the mixtures are pre-treated using the seepage tests illustrated in the right part of this figure).

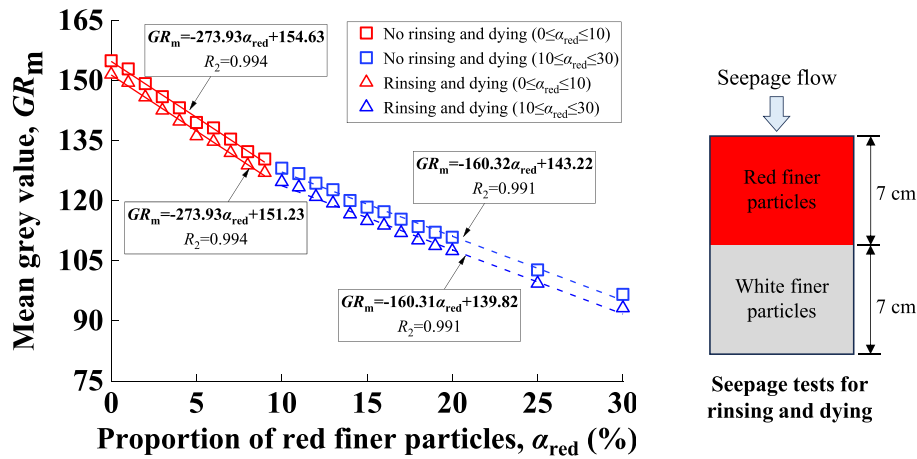


**Fig. 9.** Flow chart for determining the proportion of finer red particles in the mixture of finer red and white particles.

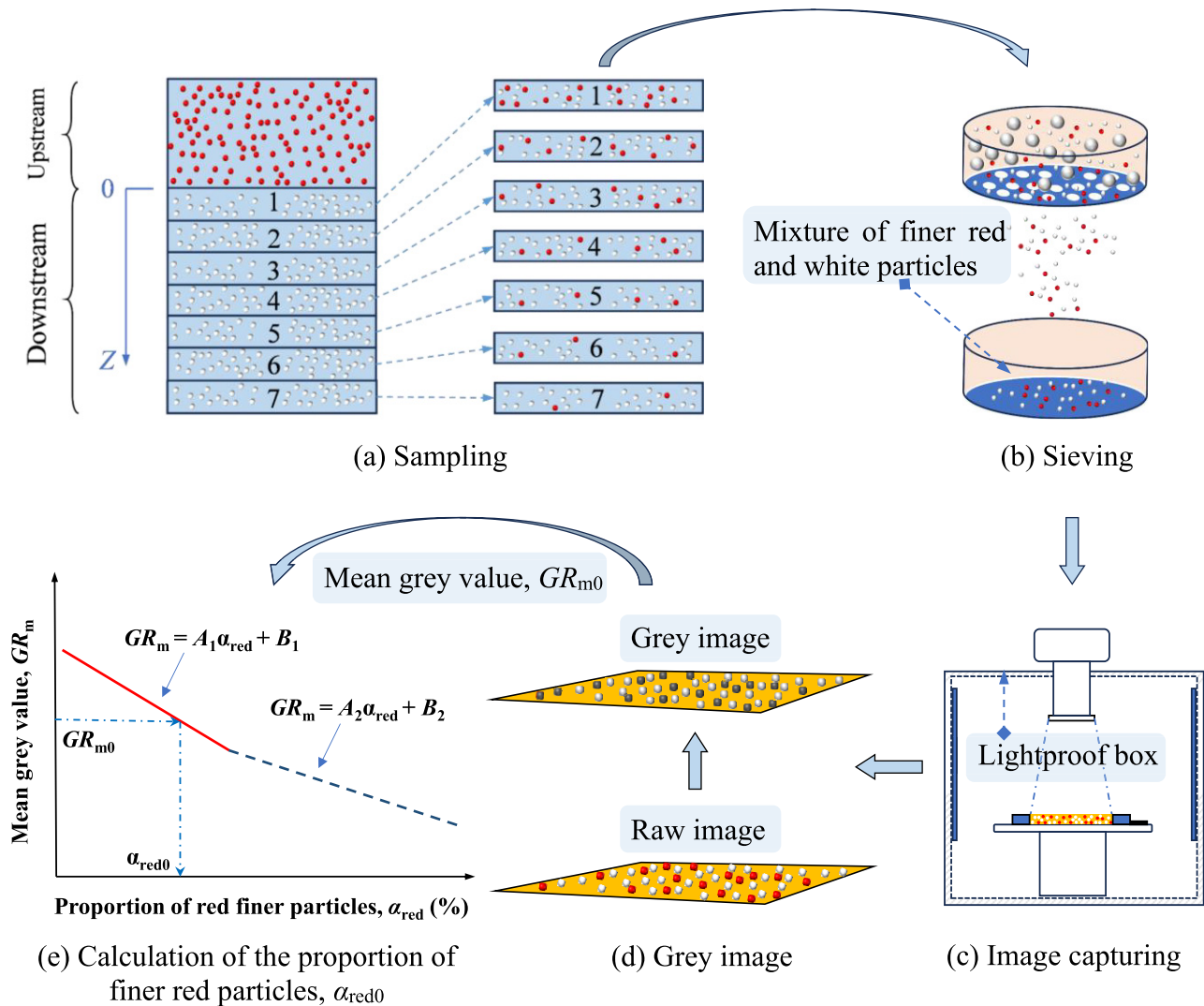
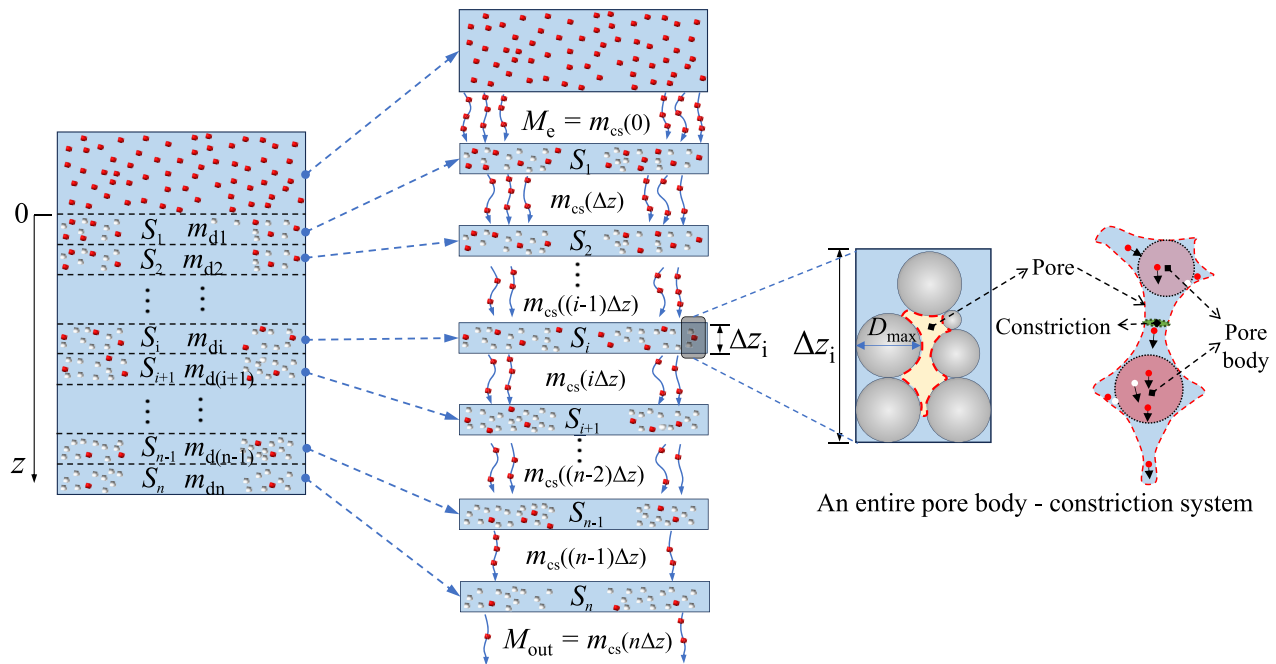




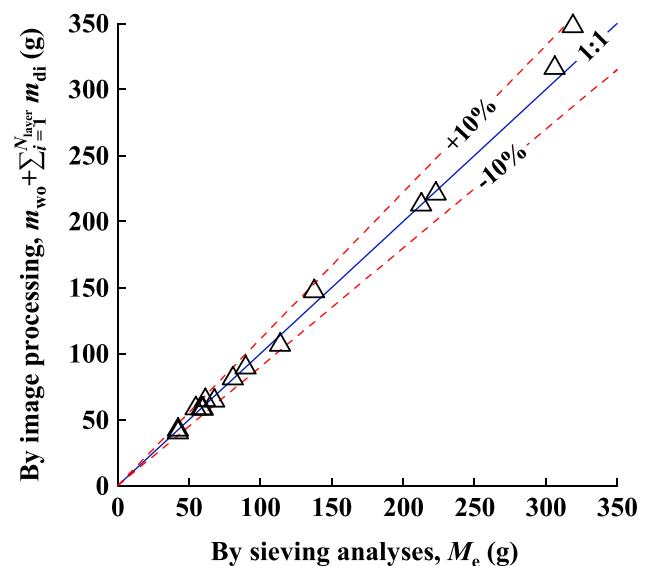
**Fig. 10.** Schematic illustrating the movement of finer red particles: washed-out from the upstream soil column ( $M_e$ ) and deposition within the downstream soil column (in which  $m_{di}$  stands for the mass of finer red particles redeposited within the  $i$ th sublayer,  $S_i$ , of the downstream soil column;  $m_{cs}((i-1)\Delta z)$  is the mass of finer red particles passing through the top surface cross section of  $S_i$ , in which  $(i-1)\Delta z$  represents the  $z$  coordinate of the top surface of  $S_i$ ;  $M_{out}$  is the mass of the finer red particles washed out from the soil column).



of the upstream soil column and subsequently deposited in each sublayer of the downstream soil column (see Fig. 10) is measured as the mass of finer red particles in the sublayer after suffusion, using the image processing-based approach detailed in Section 3. Additionally, some of the eroded finer particles are washed out of the soil column (see Fig. 10) and collected in the particle collection system (see Fig. 2). These collected particles are typically a mixture of finer red and white particles, as the finer particles both in the upstream and downstream soil columns may be washed out. Similarly, the mass,  $m_{wo}$ , of the finer red particles collected in the particle collection system is measured using the image processing-based approach described in Section 3.

Ideally, the total mass,  $M_e$ , of the finer particles washed out from the upstream soil column should equal the sum of the total mass,  $\sum_{i=1}^{N_{layer}} m_{di}$ , of the finer red particles deposited in each layer of the downstream soil column and the mass,  $m_{wo}$ , of the finer red particles collected in the particle collection system. This relationship serves as a reference to assess the accuracy of the image processing-based approach. The relative error,  $\frac{(m_{wo} + \sum_{i=1}^{N_{layer}} m_{di}) - M_e}{M_e}$ , is generally within  $\pm 5\%$  for most experimental tests, although in some cases, it ranges from  $\pm 5\%$  to  $\pm 10\%$ , as shown in Fig. 11. This error may be rooted in the accuracy of sampling and sieving analyses as well as the precision of the correlation established in Fig. 8. Nevertheless, the error is considered acceptable for the purpose of this study.

**Fig. 11.** Comparison of the total mass of eroded finer particles from the upstream soil column: predicted by the newly developed image processing-based approach,  $M_e^{Pre} = (m_{wo} + \sum_{i=1}^{N_{layer}} m_{di})$ , versus measured by sieving analyses,  $M_e$ , for all suffusion tests in this study.



## 4.2. Exponential decay of $\gamma_d$ along seepage direction

The redeposition ratio per seepage length,  $\gamma_d$ , is calculated for each sublayer using eq. 1 and then plotted against the normalized seepage length,  $z/D_{\max}$  for soil samples with various contents of finer fraction,  $F_c$ , as presented in Fig. 12a; in which  $z$  represents the distance between the bottom of the upstream soil column and the midpoint of each sublayer in the downstream soil column, as illustrated in Fig. 9a.

The results indicate that the redeposition of eroded finer particles decays exponentially along the seepage direction, as indicated by the approximately linear relationship between  $\gamma_d$  and  $z/D_{\max}$  on a semi-logarithmic scale for soil samples with a broad range of contents of finer fraction,  $F_c$ , from 15% to 35% (Fig. 12a). Additionally, a comparative test, i.e., case T1, is conducted where the downstream soil column is packed with only coarser particles (i.e.,  $F_c^{\text{down}} = 0\%$ ) while the upstream soil column is packed with gap-graded soil having  $F_c^{\text{up}} = 25\%$ . In this case, the downstream redeposition of the finer particles washed out of the upstream soil column could be easily quantified using the sieving analyses. The results show an exponential decay in redeposition along the seepage direction, similar to the cases where the downstream soil columns are packed with gap-graded soils (i.e.,  $F_c = 15\text{--}35\%$ ). It is noteworthy that case T1 is similar to the self-filtering in base soil-filter systems described in Raut and Indraratna (2008) and Locke et al. (2001). However, for other cases (T2–T21), the downstream soil columns are packed using gap-graded soils consist of both coarser and finer particles. The downstream redeposition of finer particles eroded from the upstream soil and the erosion of finer particles initially packed in the downstream soil occur simultaneously in the downstream soil, which are different from the self-filtering in base soil-filter systems.

The results shown in Fig. 12a reveal that the downstream redeposition of finer particles consistently follows an exponential decay pattern, regardless of the content of finer fractions in the downstream soil column. To test the generality of the results, we perform suffusion tests on gap-graded soils with different size ratios between the coarser and finer fractions (see Fig. 12b), applying hydraulic gradients in different ways (see Fig. 12c), and using different flowrates through the soil column (see Fig. 12d). The downstream redeposition of finer particles along the seepage direction consistently follow an exponential trend. Besides, we conduct additional experiments with an overlying soil layer (6 cm in height) placed on top of the upstream soil column, as depicted in Fig. 5. As presented in Fig. 12e, the presence of the overlying soil layer has a minimal impact on the downstream redeposition of the finer particles.  $\gamma_d$  consistently follows an exponential decay pattern, regardless of the overlying soil layer. This suggests that the location of the upstream soil column, whether at the top or within the soil column, has limited effect on the downward redeposition of the finer particles washed out from the soil column. In reality, the content of finer fraction can differ between the upstream and downstream soils. Therefore, we further considered situations in which the upstream and downstream soil columns have different initial contents of

finer fraction, i.e.,  $F_c^{\text{up}}$  and  $F_c^{\text{down}}$ , respectively. For this purpose, we tested nine soil samples with various combinations of  $F_c^{\text{up}}$  and  $F_c^{\text{down}}$ , specifically at 15%, 25%, and 35%, and the results are presented in Fig. S3 of Supplementary Information. The redeposition of finer particles is affected by the content of finer fraction in the upstream soil column. Despite different finer fraction between the upstream and downstream soil columns, the redeposition of finer particles still follows an exponential decay pattern.

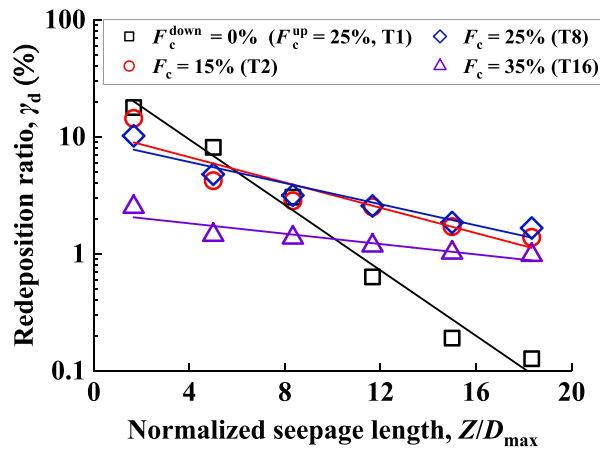
In summary, it can be concluded that although the redeposition ratio differs across various situations, the exponential decay behaviour remains unchanged. The impact of these factors on the redeposition of finer particles will be investigated in Section 6. It is noteworthy that the exponential decay of redeposition does not necessarily mean that most of the eroded finer particles from the upstream soil column would escape from the downstream soil skeleton. To clarify this, we calculate the total redeposition ratio  $\Gamma_d = M_d/M_e$  in the downstream soil column for each test, as listed in Table S4 of the Supplementary Information, in which  $M_e$  is the total mass of the finer particles eroded from the upstream soil column and  $M_d$  is the total mass of the finer particles eroded from the upstream soil column and then redeposited in the downstream soil column. For the downstream soil column with relatively small finer fraction (e.g., T1–T4,  $F_c = 0\text{--}15\%$ ), most (>90%) of the eroded finer particles are redeposited in the downstream soil column, indicating that a very small proportion (<10%) of the eroded finer particles pass through and escape from the downstream soil skeleton. While for the downstream soil column with relatively large finer fraction (e.g., T16–T19,  $F_c = 35\%$ ), a relatively large proportion (60%–70%) of the eroded finer particles escape from the downstream soil skeleton. Nevertheless, there is still a certain amount (30%–40%) of eroded finer particles redeposited within the downstream soil skeleton.

## 5. Theoretical analyses for the exponential decay of $\gamma_d$

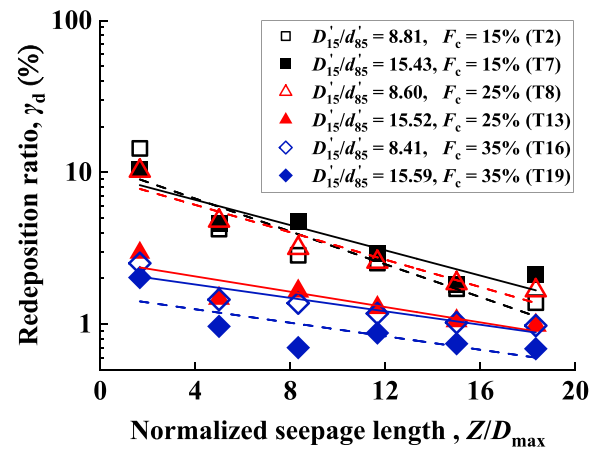
### 5.1. Theoretical derivation of $\gamma_d$ based on the redeposition probability

To have an insight into the exponential decay of  $\gamma_d$ , a theoretical model is developed to describe the decay of  $\gamma_d$  along the seepage direction. To this end, the downstream soil column is divided into equally sized sections, termed  $S_i$ , with a thickness of  $\Delta z$ , as illustrated in Fig. 10. The finer red particles are washed out from the upstream soil column and progressively transported through the subsequent sections,  $S_i$ , of the downstream soil column. Let  $m_{cs}(z)$  represent the mass of the finer red particles passing through a cross-section at coordinate  $z$  within the downstream soil column. Consequently, the mass of finer red particles entering section  $S_i$  is the mass of the finer red particles passing through the top surface cross-section of  $S_i$ , which is  $m_{cs}((i-1)\Delta z)$ , where  $(i-1)\Delta z$  is the  $z$ -coordinate of the top surface of  $S_i$  (see Fig. 10). It follows that  $m_{cs}((i-1)\Delta z)$  decreases with the increasing  $i$  since the finer red particles are gradually redeposited as they move down-

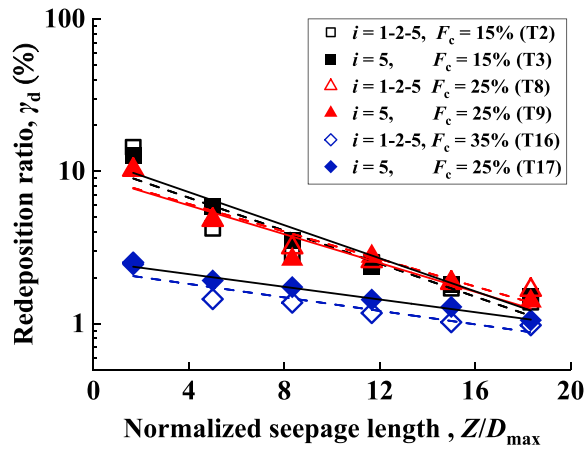
**Fig. 12.** Decay of the redeposition ratio per seepage length,  $\gamma_d$ , along the seepage direction for different initial contents of finer fraction,  $F_c$ , different size ratios,  $D_{15}'/d_{85}'$ , different manners for applying the hydraulic gradient, different flowrates,  $Q_w$ , and soil columns with/without overlying soil layers (in which the contents of finer fraction,  $F_c$ , are the same for both the upstream and downstream soil columns unless otherwise stated;  $F_c^{\text{down}}$  and  $F_c^{\text{up}}$  stand for the finer fraction of the downstream and upstream soil column, respectively).



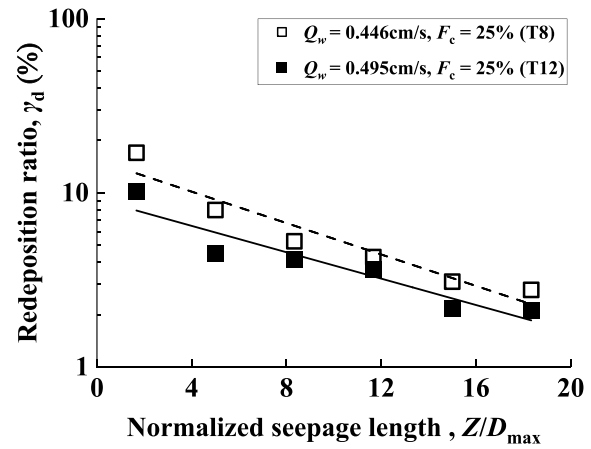
(a) Different finer fractions,  $F_c$



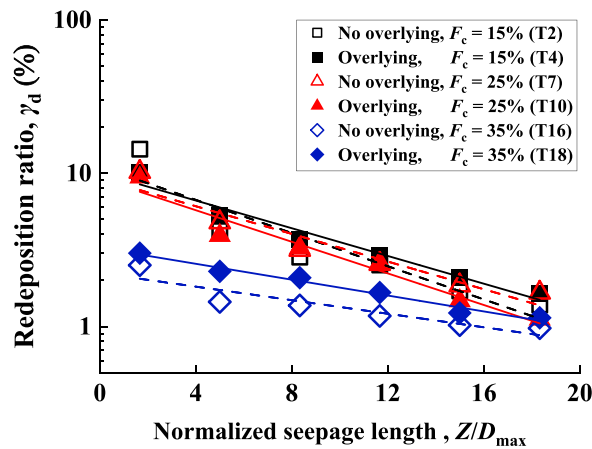
(b) Different size ratios,  $D_{15}'/d_{85}'$



(c) Applying of hydraulic gradients



(d) Different flowrates,  $Q_w$



(e) Overlying soil layers

ward. On the other hand, the mass of the finer red particles entering the first section  $S_1$ , i.e.,  $m_{cs}(0)$  is equal to the total mass,  $M_e$ , of the finer red particles washed out from the upstream soil column.

Given that the washed-out finer red particles would be partially redeposited in each section  $S_i$ , a redeposition probability per seepage length,  $P_{di}$ , is defined for each section  $S_i$  as follows:

$$(2) \quad P_{di} = \frac{m_{di}/m_{cs}|_{z=(i-1)\Delta z}}{\Delta z}$$

where  $z = (i-1)\Delta z$  denotes the  $z$ -coordinate of the top surface of  $S_i$ ;  $m_{di}$  is the mass of the finer red particles deposited within each section  $S_i$ . Note that  $P_d$  is analogous to the concept of probability density.

Considering the mass conservation for finer red particles entering a section  $S_i$ , the following mass balance equation is derived:

$$(3) \quad m_{cs}|_{z=i\Delta z} = m_{cs}|_{z=(i-1)\Delta z} - m_{di}$$

According to this mass balance equation (eq. 3), the mass of the finer red particles entering the  $S_{(i+1)}$  section (i.e., passing through the top surface cross-section of  $S_{(i+1)}$ ), which is  $m_{cs}|_{z=i\Delta z}$  where  $z = i\Delta z$  is the  $z$ -coordinate of the top surface of  $S_{(i+1)}$ , is related to the total mass,  $M_e$ , of the finer red particles washed out from the upstream soil column and the mass,  $m_{di}$ , of the finer red particles deposited within each section as follows:

$$(4) \quad m_{cs}|_{z=i\Delta z} = M_e - \sum_{j=1}^i m_{dj}$$

By substituting eq. 2 into eq. 4, we get

$$(5) \quad m_{cs}|_{z=i\Delta z} = M_e - \sum_{j=1}^i (m_{cs})|_{z=(j-1)\Delta z} P_{dj} \Delta z$$

As  $\Delta z$  approaches a very small value, eq. 5 can be re-expressed in an integral form as follows:

$$(6) \quad m_{cs}(z) = M_e - \int_0^z m_{cs}(\lambda) P_d(\lambda) d\lambda$$

in which  $\lambda$  is an integration variable. Differentiating both sides of eq. 6 with respect to  $z$ , we obtained a first-order ordinary differential equation for  $m_{cs}(z)$ , as follows:

$$(7) \quad \frac{dm_{cs}(z)}{dz} + P_d(z) m_{cs}(z) = 0$$

Solving eq. 7 provides the mass,  $m_{cs}(z)$ , of finer red particles passing through the cross section at coordinate  $z$  within the downstream soil column:

$$(8) \quad m_{cs}(z) = C e^{-\int P_d(z) dz}$$

where  $C$  is an integration constant. Substituting eq. 8 into eq. 2, the mass,  $m_d(z)$ , of redeposited finer red particles within each sublayer of the downstream soil column is related to the redeposition probability per seepage length,  $P_d(z)$ , as follows:

$$(9) \quad m_d(z) = C P_d(z) e^{-\int P_d(z) dz} \Delta z$$

Considering the definition of the redeposition ratio per seepage length,  $\gamma_d$ , i.e.,  $\gamma_d = \frac{m_d/M_e}{\Delta z}$ ,  $\gamma_d(z)$  is related to  $P_d(z)$  according to eq. 9, as follows:

$$(10) \quad \gamma_d(z) = \frac{C}{M_e} P_d(z) e^{-\int P_d(z) dz}$$

Equation 10 indicates that  $\gamma_d$  exhibits an exponential-like decay along the seepage direction. The exact form of this decay depends on the variation of the redeposition probability per seepage length,  $P_d(z)$ , along the seepage direction. This relationship will be explored in the following section:

## 5.2. Variation of redeposition probability along the seepage direction

The redeposition probability per seepage length,  $P_d$ , of the finer red particles deposited within the sublayers of the downstream soil column (see Fig. 9a) is calculated using the experimental data as follows:

$$(11) \quad P_{di} = \frac{m_{di}/(M_e - \sum_{j=0}^{i-1} m_{dj})}{(\Delta z_i/D_{\max})}$$

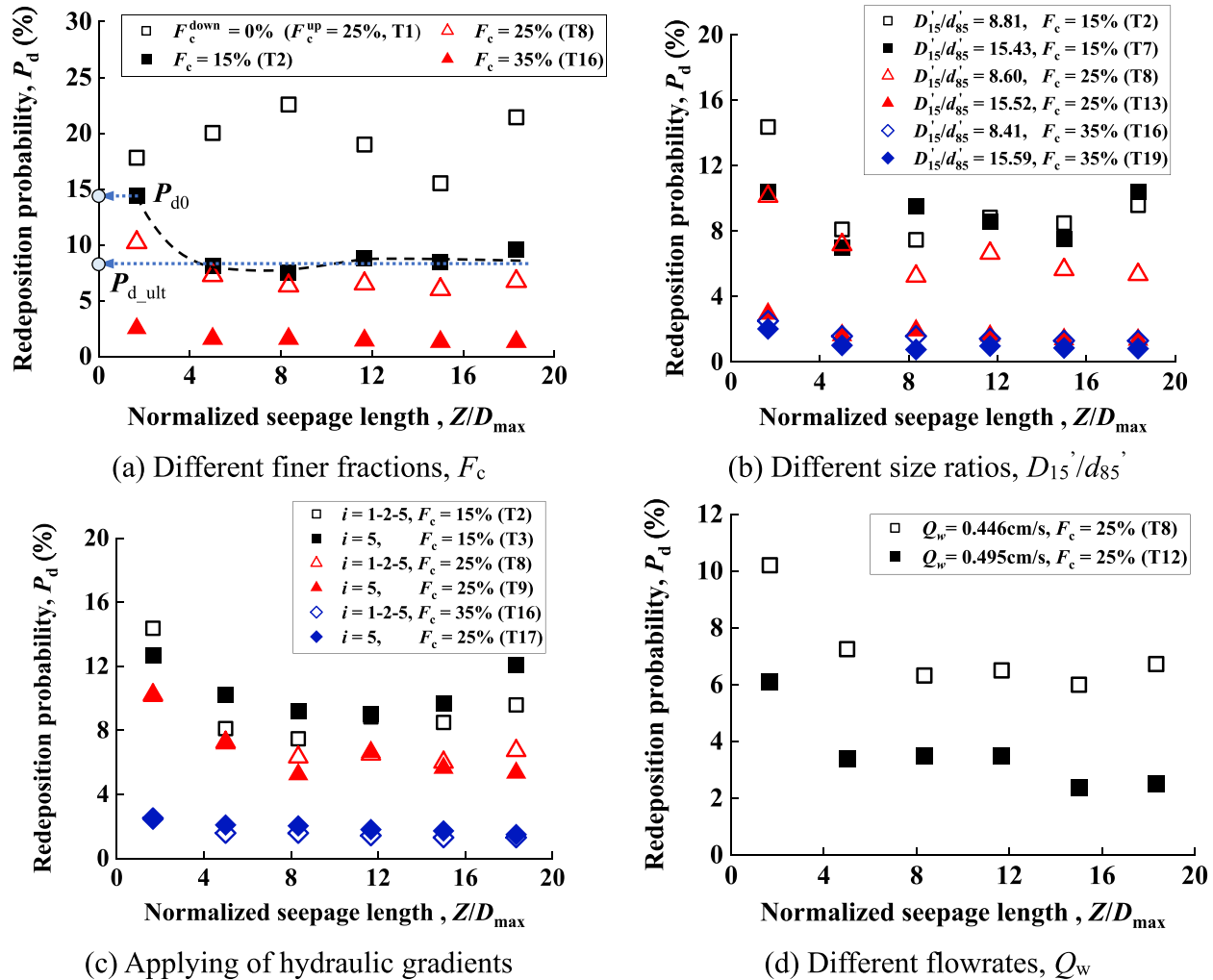
in which  $m_{di}$  and  $m_{dj}$  denote the mass of the finer red particles deposited in the  $i$ th and  $j$ th sublayers, respectively, as measured using the proposed image processing-based approach as detailed in Section 3.2.  $m_{d0}$  is defined as zero.

The variation in the redeposition probability per seepage length,  $P_d$ , is obtained along the seepage direction for different contents of finer fraction,  $F_c$ , as presented in Fig. 13a. For the sample with  $F_c^{\text{down}} = 0\%$  (i.e., the downstream soil column contains only coarser particles),  $P_d$  fluctuates around a relatively constant value along the seepage direction. In contrast, for soil samples with  $F_c = 15\%-35\%$ ,  $P_d$  initially decreases, then the rate of decrease slows. It eventually approaches a constant value. The initial decrease in  $P_d$  should be attributed to the occupation of preferential deposition positions by finer particles eroded from adjacent soil sublayers, which will be detailed in Section 8. The adjacent occupation can limit the redeposition of the finer red particles (eroded from the upstream soil column) within the downstream soil column, except in the uppermost sublayer, where there is no adjacent occupation since its upstream side is adjacent to the upstream soil column. For the sample with  $F_c^{\text{down}} = 0\%$ , there is no adjacent occupation since the downstream soil column contains no finer particles. Consequently, no significant initial decrease in  $P_d$  is observed for this sample.

To test the generality of the results, variations in  $P_d$  along the seepage direction are examined for samples with different size ratios between the coarser and finer fractions (see Fig. 13b), as well as for samples tested with different



**Fig. 13.** Variation of redeposition probability per seepage path,  $P_d$ , along the seepage direction for different contents of finer fraction,  $F_c$ , different size ratios,  $D_{15}'/d_{85}'$ , different hydraulic gradient application methods, and different flowrates,  $Q_w$ .



methods of applying the hydraulic gradient (see Fig. 13c) and varying flowrates through the soil column (see Fig. 13d). In these cases, the variations in  $P_d$  along the seepage direction show a similar pattern:  $P_d$  initially decreases within  $2-4D_{max}$  along the seepage direction and then approximately levels off. Meanwhile, we also noticed several exceptions. One is the sample with  $F_c = 15\%$  and a relatively large size ratio,  $D_{15}'/d_{85}' = 15.43$  (i.e., T7 in Fig. 13b). This sample exhibits a relatively large fluctuation in redeposition probability along the seepage direction, similar to the behaviour observed in the sample with downstream soil columns packed exclusively with coarser particles (i.e., T1 in Fig. 13a). This behaviour should be attributed to the very loose packing of finer particles within the voids of the coarse skeleton for the T7 sample with relatively small  $F_c$  and large size ratio. The other one is the test T3 (in which  $i = 5$  and  $F_c = 15\%$ ) in Fig. 13c, in which an abnormal increase after  $Z/D_{max} = 12$  is observed. This should be attributed to a random fluctuation, which is similar to that in the sample with no finer particles in the downstream soil column (i.e., T1 in Fig. 13a), as well as in the sample with a relatively large gap (i.e., T7 in Fig. 13b).

### 5.3. Derivation of the exponential decay of $\gamma_d$ based on the variation of redeposition probability

The precise form of the decay of the redeposition ratio per seepage path,  $\gamma_d$ , depends on the variation of the redeposition probability per seepage length,  $P_d(z)$ , along the seepage direction, as given by eq. 10. As previously noted,  $P_d$  initially decreases along the seepage direction, then the rate of decrease diminishes, and eventually  $P_d$  approaches a constant value within the downstream sublayers approximately  $2-4D_{max}$  from the upstream soil column. That is to say, the redeposition probability is nearly constant over most of the seepage path. The derivation of the theoretical model is based on this assumption. Note that this assumption is obtained in the experimental tests on uniformly packed soils columns under 1D seepage (see Fig. 13). However, it is not always valid in real-world scenarios since the soils may be nonuniform along the seepage path. Nevertheless, the nonuniform soils could be treated as piecewise uniform along the seepage path in many situations. Therefore, the theoretical model based on constant redeposition probability assumption may be ap-

plied individually to each uniform soil column, although the soils may be nonuniform along the seepage path. However, further studies are still needed for the validation of the theoretical model in nonuniform soil columns, which will be considered in our future study. On the other hand, the seepage path may converge or diverge in real-life dam foundations and slopes while it is always parallel in the current tests. The converging or diverging of the seepage path should have important influence on the redeposition probability while it is not considered in the current study. Therefore, the assumption of constant redeposition probability and the associated theoretical model are only applicable to the situations with parallel seepage paths.

To simplify the derivation of  $\gamma_d$ , the process is conducted in two phases. First,  $P_d(z)$  is approximated as constant along the seepage direction to simplify eq. 10. Subsequently, additional parameters are incorporated into this simplified expression to account for the initial decrease in  $P_d(z)$  along the seepage direction. It should be acknowledged that this approach may introduce some deviation, which will be examined in the final part of Section 5.

Assuming  $P_d(z)$  is constant and denoted as  $P_{d0}$  in eqs. 8 and 10, these equations can be simplified as follows:

$$(12) \quad m_{cs}(z) = Ce^{-P_{d0}z}$$

$$(13) \quad \gamma_d(z) = \frac{C}{M_e} P_{d0} e^{-P_{d0}z}$$

Given that  $m_{cs}(0) = M_e$ , the constant  $C$  is determined to be equal to  $M_e$  according to eq. 12. Consequently, the expression for  $\gamma_d(z)$  (i.e., eq. 13) can be further simplified to

$$(14) \quad \gamma_d(z) = P_{d0} e^{-P_{d0}z}$$

Equation 14 indicates an exponential decay of the redeposition ratio,  $\gamma_d$ , along the seepage direction.

Subsequently, an additional parameter is introduced into the expression for  $\gamma_d(z)$  (eq. 14) to account for the variation in  $P_d$  along the seepage direction, as observed in the experimental tests (see Fig. 13). Specifically, a parameter  $\alpha$  is incorporated into eq. 14 as follows:

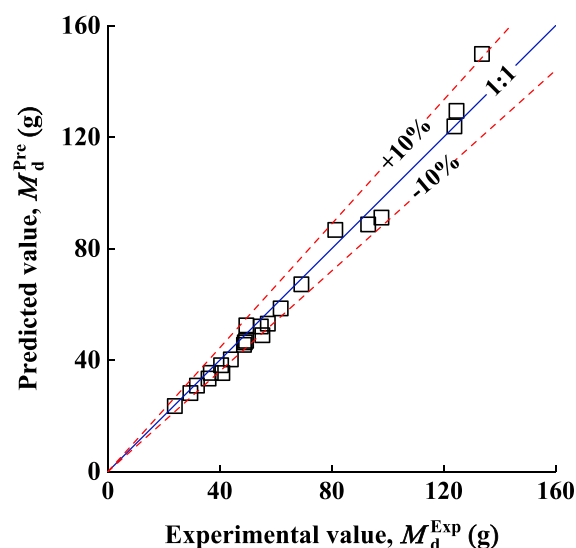
$$(15) \quad \gamma_d(z) = P_{d0} e^{-\alpha P_{d0}z}$$

The parameter  $\alpha$  reflects the variation in  $P_d(z)$  within the downstream soil column. Additionally, as  $z$  approaches zero, the deposition rate per seepage path,  $\gamma_d(z \rightarrow 0)$  approaches the deposition probability per seepage path,  $P_d(z \rightarrow 0)$ , based on the definitions of  $\gamma_d$  (eq. 1) and  $P_d$  (eq. 11); note that  $z \rightarrow 0$  indicates  $\sum_{j=0}^{i-1} m_{dj} = 0$  in eq. 11. Furthermore,  $\gamma_d(z \rightarrow 0)$  equals  $P_{d0}$  according to the eq. 15. This implies that  $P_{d0}$  equals  $P_d(z \rightarrow 0)$ , meaning that  $P_{d0}$  represents the redeposition probability per seepage length within the uppermost downstream sublayer. Hereafter,  $P_{d0}$  will be referred to as the original deposition probability per seepage length.

#### 5.4. Examination on the validity of eq. 15

The parameters  $P_{d0}$  and  $\alpha$  are determined by fitting eq. 15 to the experimental data for the variation of  $\gamma_d$  with  $z$  (see Fig. 12). The fitted parameters are listed in Table S5 of the

**Fig. 14.** Comparison between the total mass,  $M_d^{\text{Pre}}$ , of the finer red particles deposited within the downstream soil column predicted using eq. 15 and those measured in the experimental tests.



Supplementary Information, and typical fitted curves are presented in Fig. S4 of the Supplementary Information. It can be seen that eq. 15 provides a reasonable fit to the experimental results. Meanwhile, it should be acknowledged that the redeposition near the inlet of the downstream soil column (i.e., within the range  $z/D_{\text{max}} = 0-2$ ) is underestimated. This is because the initial reduction in redeposition probability (see Fig. 13) could not be fully captured by the parameter  $\alpha$  in eq. 15.

For a further validation, eq. 15 with the fitted parameters (see Table S5 of the Supplementary Information) is used to predict the total mass,  $M_d^{\text{Pre}}$ , of the finer red particles redeposited within the downstream soil column as follows:

$$(16) \quad M_d^{\text{Pre}} = M_e \int_0^{L/D_{\text{max}}} \gamma_d(\lambda) d\lambda$$

where  $L$  is the total length of the downstream soil column;  $M_e$  is the total mass of the finer red particles washed out from the upstream soil column, determined through sieving analysis as described in Section 4.1.  $M_d^{\text{Pre}}$  is compared to the experimentally measured mass of redeposited finer red particles within the downstream soil column, termed  $M_d^{\text{Exp}}$ . As shown in Fig. 14, the predicted mass  $M_d^{\text{Pre}}$  is generally close to experimentally measured mass  $M_d^{\text{Exp}}$  with relative errors typically not exceeding 10%. It confirms the validity of eq. 15.

## 6. Effect of content of finer fraction on the redeposition probability

The redeposition probability per seepage length,  $P_d$ , is a crucial quantity that influences the downstream redeposition of finer particles washed out from the upstream soil skeleton, as indicated by eq. 15. It is expected to be closely related

to the content of finer fraction,  $F_c$ , as indicated by Fig. 13. This will be explored further in this section. Note that  $P_d$  exhibits some variations along the downstream soil column in each test, as depicted in Fig. 13. Therefore, two distinct characteristic redeposition probabilities are considered: the original redeposition probability per seepage length,  $P_{d0}$ , and the ultimate redeposition probability per seepage length,  $P_{d_{ult}}$ , as illustrated in Fig. 13a; here,  $P_{d_{ult}}$  is defined as the mean value of the redeposition probabilities per seepage length over the sublayers located  $4D_{max}$  away from the interface between the upstream and downstream soil columns (note that  $P_d$  approximately becomes constant in these sublayers, which are  $4D_{max}$  away from the interface).

The effects of the content of finer fraction in the upstream and downstream soil columns, denoted as  $F_c^{up}$  and  $F_c^{down}$ , on redeposition probabilities are investigated. The two characteristic redeposition probabilities per seepage length,  $P_{d0}$  and  $P_{d_{ult}}$ , are determined for soil samples with varying  $F_c$ , as shown in Fig. 15a; note that the  $F_c^{down}$  in the downstream soil column may differ from  $F_c^{up}$  in the upstream column, while the redeposition probabilities are plotted against the  $F_c^{down}$  by default.

Figure 15a reveals that both the  $P_{d0}$  and  $P_{d_{ult}}$  significantly decrease with the increment of the content of finer fraction in the downstream soil column, regardless of the  $F_c^{up}$ . It indicates that the finer particles washed out from the upstream soil column are less likely to be redeposited in the downstream soil column with a higher content of finer fraction. This observation seems to be counterintuitive, as a higher content of finer fraction typically implies a denser packing of finer particles within the coarse matrix, which should have been expected to create more resistance to the passage of fluidized/eroded finer particles, thus enhancing their redeposition. To verify the reliability of these results, additional testing conditions are considered.

One such condition is the water flowrate, which is addressed in Fig. 15b. Note that soils with a higher content of finer fraction typically have lower hydraulic conductivities, resulting in generally lower water flowrates. Water flow with a lower flowrate has a reduced capacity to transport fluidized/eroded finer particles, which consequently enhances the redeposition of the particles, leading to a higher redeposition probability, as shown in Fig. 15b. This suggests that the observed decrease in redeposition probability with the increasing  $F_c$  would be more pronounced if the water flowrate were consistent across all experimental tests with different  $F_c$  values.

Additionally, results for gap-graded soils with varying size ratios between the coarser and finer fractions,  $D_{15}/d_{85}'$ , are presented in Fig. 15c. Generally, a larger size ratio,  $D_{15}/d_{85}'$ , is associated with a lower redeposition probability. This is because a larger size ratio generally signifies a reduced resistance to the migration of eroded finer particles through the pores of the downstream soil column, due to the larger constriction sizes of the coarse matrix relative to the diameter of the finer fraction. Notably, the observed decrease in redeposition probability with the increasing  $F_c$  persists at larger size ratios between the coarser and finer fractions.

Furthermore, different methods of applying hydraulic gradients (including step-wised and constant hydraulic gradients) and the presence of overlying soil layers above the upstream soil column (see Fig. 5) are considered. As shown in Figs. 15d and 15e, variations in redeposition probabilities with  $F_c$  are found to be largely unaffected by the hydraulic gradient applying methods and the presence of overlying soil layers.

In summary, the redeposition probability generally exhibits a decreasing trend with the increasing content of finer fraction,  $F_c$ , under various testing conditions. To further understand this phenomenon, the concept of preferential deposition position is introduced and discussed in Section 7.

## 7. Preferential deposition position: concept and its relation to redeposition probability

Firstly, we investigate the redeposition positions of the finer red particles within the downstream soil column. To achieve this, cross-sectional images of soil samples with varying  $F_c$  are captured after suffusion, as presented in Fig. 16.

The images reveal that the redeposition of finer red particles is relatively homogeneous in the cross-section of soil samples with  $F_c = 15\%$ , while they exhibit significant localization within specific regions in the soil samples with  $F_c = 35\%$ . The degree of homogeneity and localization of the finer red particles is quantified using the nearest neighbour analysis (NNA) (Clark and Evans 1954), specifically through the average nearest neighbour ratio,  $r_{ann}$  presented in Fig. 16. Detailed methodology for the calculation of  $r_{ann}$  is provided in Section S7 of the Supplementary Information. Typically, a smaller  $r_{ann}$  ( $<1$ ) corresponds to a more localized distribution of the redeposited finer red particles within the cross-section, as illustrated in Fig. S5 of the Supplementary Information. These results offer quantitative evidence that the channels for the transportation and redeposition of the finer red particles become more localized as the content of finer fraction,  $F_c$ , increases.

We further propose that certain positions within the voids of the coarse skeleton facilitate the redeposition of finer particles, as illustrated in Fig. 17. These positions are referred to as preferential redeposition positions. It should be noted that the theoretical concept of preferential redeposition position is a hypothesis used to explain the observations in the current study which will be detailed below.

The number of such preferential deposition positions in a given coarse skeleton is assumed to be approximately constant, provided that other conditions, such as the finer particle diameter and the water flowrate, remain unchanged. From this perspective, a homogeneous distribution of the channels for transporting and redepositing the finer particles in the downstream soil columns with  $F_c = 15\%$  (observed in the experiments as shown in Fig. 16) suggests a higher likelihood of these particles being transported to and redeposited at these preferential positions, compared to the

**Fig. 15.** Variation of the original redeposition probability per seepage length,  $P_{d0}$ , and the ultimate deposition probability per seepage length,  $P_{d_{ult}}$  with the content of finer fraction,  $F_c$ , under various testing conditions, including different  $F_c^{down}$  and  $F_c^{up}$ , different size ratios,  $D_{15}'/d_{85}'$ , different methods of applying hydraulic gradients, the presence or absence of overlying soil layers above the upstream soil column (in which  $F_c^{down}$  and  $F_c^{up}$  stand for the content of finer fraction in the downstream and upstream soil columns, respectively).

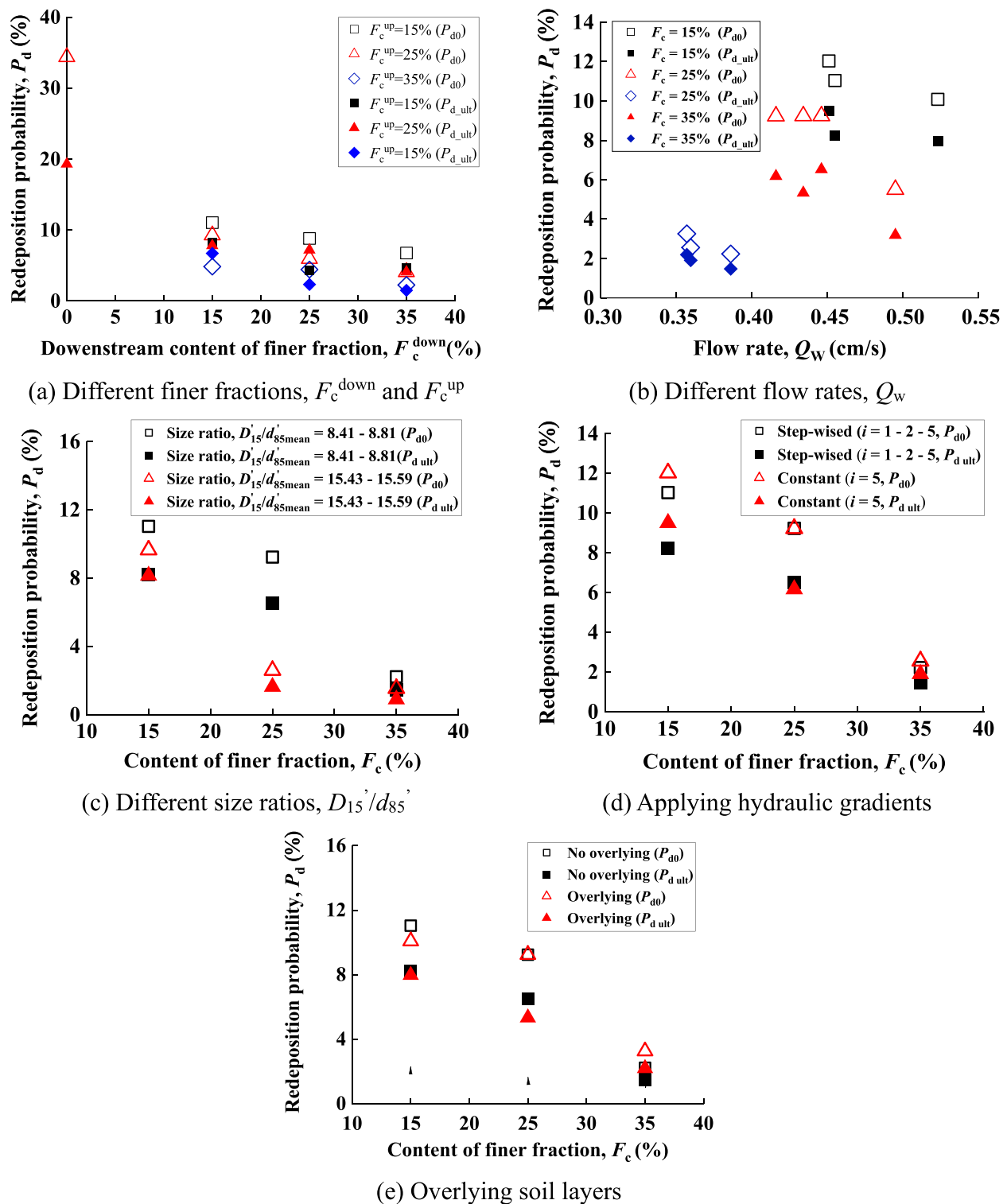




**Fig. 16.** Homogenization and localization of redeposition positions of finer red particles within typical cross-sections of soil columns with varying contents of finer fraction,  $F_c$  (in which two representative cross-sections at different heights in the downstream soil column, i.e.,  $z/D_{\max} = 8.3$  and  $11.7$ , are considered. The average nearest neighbour ratio,  $r_{\text{ann}}$ , is used to quantify the homogenization and localization, with detailed calculations provided in Section S7 of the Supplementary Information).

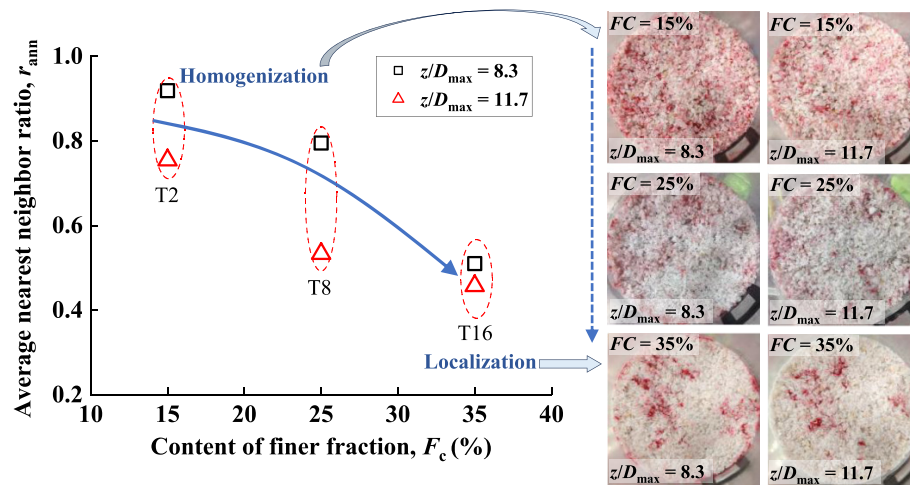
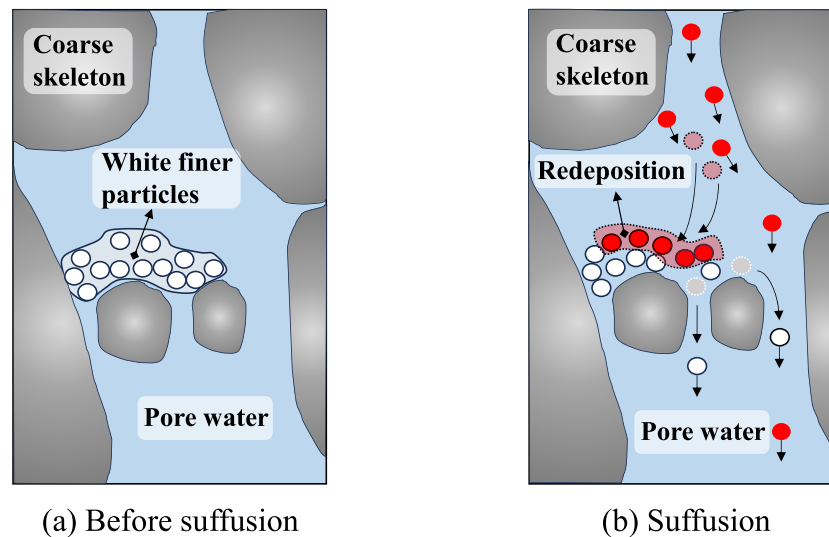


**Fig. 17.** Schematic for redeposition of finer particles within coarse skeleton voids.



more localized distributions of channels observed in the downstream soil columns with  $F_c = 35\%$  (observed in the experiments as shown in Fig. 16), as illustrated in Fig. 18. Consequently, the redeposition probability decreases with the increasing content of finer fraction,  $F_c$ , as presented in Fig. 15.

On the other hand, in downstream soil columns with a relatively high  $F_c$ , such as  $F_c = 35\%$ , most of the preferential redeposition positions within the voids of the coarse skeleton are initially occupied by finer particles already packed in these voids. Therefore, downstream soil columns with a higher  $F_c$ , such as  $F_c = 35\%$ , should have fewer available positions for the redeposition of finer particles washed out from the upstream soil columns, which may also lead to a lower redeposition probability compared to those with a lower  $F_c$ , such as  $F_c = 15\%$  (see Fig. 15).

## 8. Discussion on the initial decrease of $P_d$ along the seepage direction: insights from preferential deposition position

The initial decrease in  $P_d$  along the seepage direction (see Fig. 13) should be closely related to the occupation of preferential deposition positions by finer particles eroded from adjacent soil sublayers. In the interior soil sublayers of the downstream soil column (i.e., those not adjacent to the upstream soil column; see Fig. 19a), finer particles eroded from neighboring sublayers may occupy some preferential deposition positions within these interior soil sublayer (see Fig. 19b). This occupation impedes the redeposition of finer particles washed out from the upstream soil column (Fig. 19c), a

**Fig. 18.** Schematic of preferential deposition positions in soil samples with different contents of finer fraction,  $F_c$  (note that the illustrations of homogeneous and localized channels, respectively, for  $F_c = 15\%$  and  $35\%$  are observations in the experiments as shown in Fig. 16).

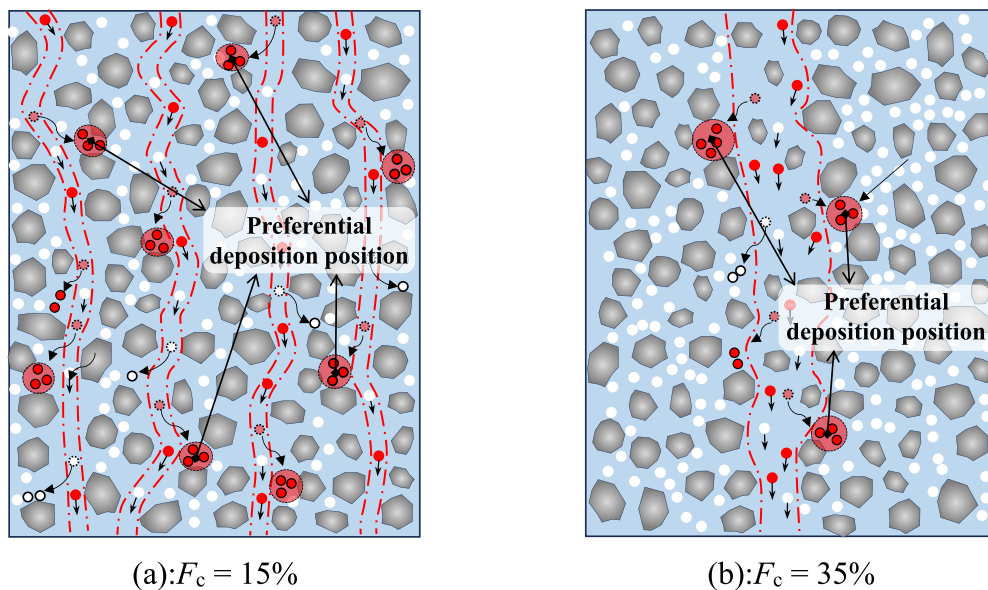
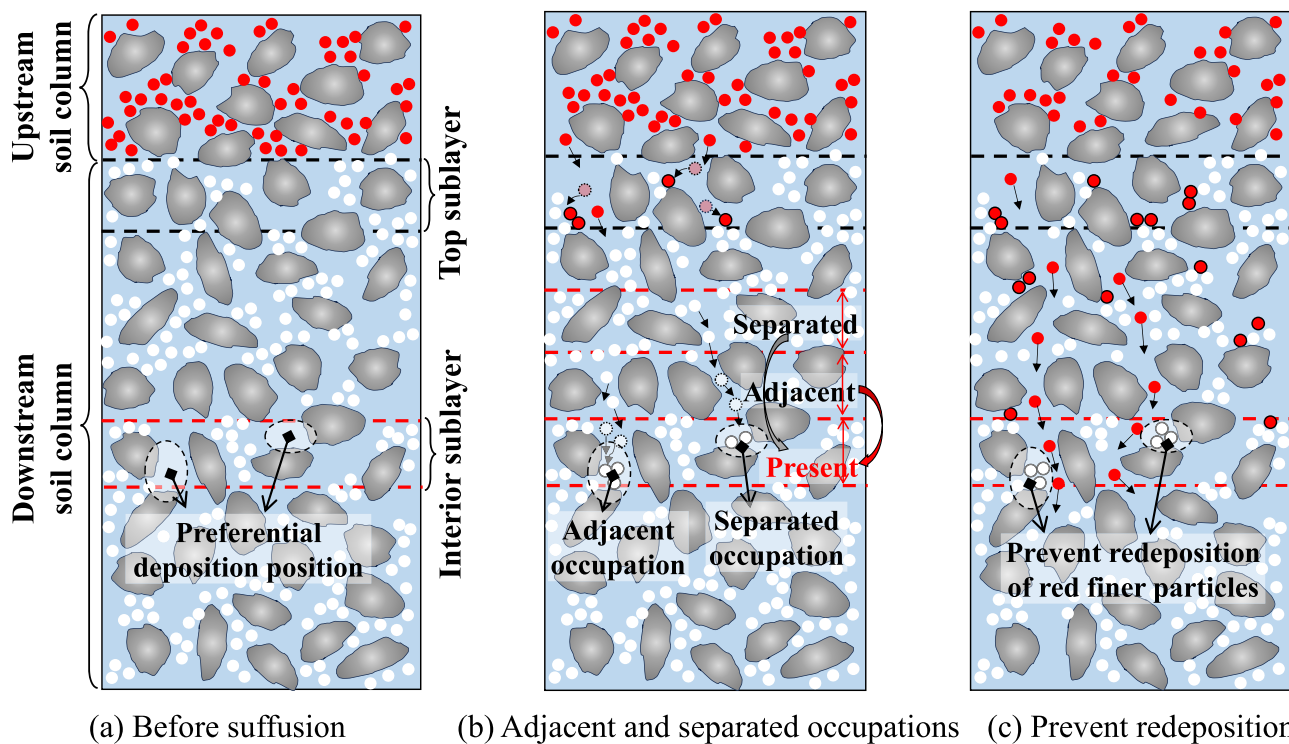


**Fig. 19.** Illustration of adjacent and separated occupation effects in the downstream soil column.



phenomenon referred to as adjacent occupation effect within the downstream soil column.

Conversely, in the top soil sublayer of the downstream soil column (i.e., the sublayer adjacent to the upstream soil column; see Fig. 19a), only finer particles washed out from the upstream soil column are redeposited. This sublayer is unaffected by the adjacent occupation effect. Consequently, finer

particles washed out from the upstream soil column have a higher redeposition probability in the top soil sublayer compared to interior soil sublayers, contributing to the initial decrease in  $P_d$  along the seepage direction, as presented in Fig. 13.

It should be acknowledged that, in an interior soil sublayer of the downstream soil column, finer particles eroded

from nonadjacent sublayers of the downstream soil column (e.g., separated by one or more sublayers; see Fig. 19b) may also occupy some of the preferential deposition positions within the current sublayer. This is termed as the separated occupation effect. Typically, the separated occupation effect should be more pronounced in lower sublayers due to greater number of separated sublayers above it. However, the separated occupation effect should be much weaker than the adjacent occupation effect, as a large proportion of finer particles eroded from the separated soil sublayers are redeposited before reaching the current sublayer, as indicated by the exponential decay of redeposition ratio (Fig. 12). Thus,  $P_d$  in interior sublayers of the downstream soil column should be primarily affected by the adjacent occupation effect rather than the separated occupation effect. Since the adjacent occupation effect should be relatively uniform across different interior sublayers, the decrease in  $P_d$  becomes less pronounced and stabilizes to a nearly constant value within the interior soil sublayers, i.e., those  $2-4D_{\max}$  away from the upstream soil column, as shown in Fig. 13.

It is noteworthy that this study mainly focuses on the quantification of redeposition along seepage path while the role of soil microstructure and fabric in redeposition is not explored due to the limitation of the experimental technique used in the current study. The X-ray CT or micro-CT imaging (Nguyen et al. 2019; Mousavi et al. 2025) could be helpful for an insight into the microscopic mechanism of redeposition, which will be considered in the future study.

## 9. Practical implications and limitations of this study

This study is focused on the redeposition of eroded finer particles along the seepage path during suffusion, which in practice would simulate key mechanism of suffusion in dam foundations and slopes. For example, rainfall-induced suffusion in colluvial slopes generally involves the redeposition of eroded finer particles within the slope toe and the lower layer of the slope, which is critical for the slope failure (Cui et al. 2017; Lei et al. 2017; Johnston et al. 2023). The exponential decay of the redeposition (Fig. 12) suggests that most of the finer particles redeposited or clogged at the slope toe or the lower layer of the slope should come from the upstream soil layers close to the redeposition or clogging position. On the other hand, the redeposition probability is found to be decreased with the increase of the finer fraction and water flowrate (Fig. 15a). This observation could be further considered in the redeposition/clogging models (Lei et al. 2017; Yang et al. 2019; Ma et al. 2022) to have a better prediction of the suffusion development in real-life dam foundations and slopes. Notably, the seepage paths in full-scale dam foundations and slopes may be different from those considered here for simplified laboratory equipment (one-dimensional). As an example, the seepage path may converge at the toe of slopes while it is always parallel in the experimental tests. The converging of the seepage path should have important influence on the redeposition while it is not considered in the current study. Therefore, the applicability of the proposed redeposi-

tion law to the field problems should be validated further, but they can still be recommended as preliminary guides prior to detailed analysis.

## 10. Conclusions

This study primarily investigates the downstream redeposition of finer particles eroded from the upstream soil matrix during suffusion. To quantify this redeposition, an image processing-based approach is developed and integrated into the one-dimensional suffusion tests. The following conclusions can be drawn:

- (1) The image processing-based approach involves packing finer fractions of the upstream and downstream soil columns with different colored quartz sand particles, allowing for the identification of migrated and redeposited particles based on color. The proportion of the finer particles, distinguished by color, within the mixture of different colored particles is found to be piece-wise linearly correlated to the mean grey value of the mixture. This approach enables the quantification of redeposition within each sublayer of the downstream soil column.
- (2) The redeposition ratio,  $\gamma_d$ , of the eroded finer particles exhibits a typical exponential decay, i.e.,  $\gamma_d(z) = P_{d0}e^{-\alpha P_{d0}z}$ , along the seepage direction  $z$  for various soil gradations (including different finer fractions 15%–35% and different size ratios 8.41–15.59), different hydraulic conditions (including step-wise or constant hydraulic gradient and varying magnitudes of hydraulic gradients/water flowrates), and different positions of the upstream soil column (whether at the top or in the interior of the soil column).
- (3) For the downstream soil column with relatively small finer fraction (e.g.,  $F_c = 0\%$ –15%), a large proportion (>90%) of the eroded finer particles from the upstream soil are redeposited in the downstream soil column. As the  $F_c$  increases to 35%, the redeposition proportion decreases, while there is still a certain amount (30%–40%) of eroded finer particles redeposited within the downstream column.
- (4) Theoretical analyses provide insight into the exponential decay of redeposition ratio, viewing it through the lens of redeposition probability. Experimental results suggest that the redeposition probability remains roughly constant throughout the downstream soil column, except in the layer immediately adjacent to the upstream soil column (with a thickness 2–4 times the maximum diameter of the coarser particles), where it initially decreases but then experiences a slowing rate of decrease. Considering this variation in redeposition probability, the theoretical analyses deduce that the redeposition ratio decays exponentially along the seepage direction.
- (5) The redeposition probability is negatively correlated to the content of finer fraction, which stems from changes in the distribution of redeposition position. The ultimate redeposition probability decreases from around 8% to around 2% as the finer fraction increases from 15% to 35% for size ratios within the range 8.41–15.59. With the



increase of finer fraction from 15% to 35%, the distribution of redeposition position shifts from homogeneous to more localized patterns within the cross-section of the downstream soil column, as demonstrated by the results of NNA. The localization of redeposition indicates that the migration and redeposition of eroded finer particles are restricted to several localized channels, reducing their chances of reaching preferential deposition positions that are supposed to be uniformly distributed within the downstream soil column. Consequently, with a higher content of finer fraction, the redeposition probability decreases due to the more localized distribution of redeposition positions.

## Acknowledgements

This study is supported by the National Natural Science Foundation of China (grant number 52009025) and by the Australian Research Council via Discovery Projects DP190102779 (Bui), FT200100884 (Bui), and DP240102765 (Bui). The author Kuang Cheng would like to acknowledge the support by China Council Scholarship for his post-doctoral research in Monash University.

## Article information

### History dates

Received: 28 January 2025

Accepted: 3 August 2025

Accepted manuscript online: 22 August 2025

Version of record online: 16 October 2025

### Copyright

© 2025 The Authors. This work is licensed under a [Creative Commons Attribution 4.0 International License](https://creativecommons.org/licenses/by/4.0/) (CC BY 4.0), which permits unrestricted use, distribution, and reproduction in any medium, provided the original author(s) and source are credited.

### Data availability

Data generated or analyzed during this study are available from the corresponding author upon reasonable request.

## Author information

### Author ORCIDs

Ha H. Bui <https://orcid.org/0000-0001-8071-5433>

### Author notes

Ha H. Bui served as Editorial Board Member at the time of manuscript review and acceptance; peer review and editorial decisions regarding this manuscript were handled by another editorial board member.

### Author contributions

Conceptualization: KC

Data curation: XC, JM

Formal analysis: KC, HL

Funding acquisition: KC, HHB

Investigation: HL, XC, JM

Methodology: KC, HL, HHB

Validation: XC

Writing – original draft: KC, HL

Writing – review & editing: HHB

## Competing interests

The authors declare there are no competing interests.

## Supplementary material

Supplementary data are available with the article at <https://doi.org/10.1139/cgj-2025-0071>.

## References

- Annapareddy, V.S.R., Sufian, A., Bore, T., and Scheuermann, A. 2024. Quantification of spatial heterogeneity and its influence on particle migration. *Géotechnique*. In press. doi:[10.1680/jgeot.23.00083](https://doi.org/10.1680/jgeot.23.00083).
- ASTM D2487-11. 2011. Standard practice for classification of soils for engineering purposes (Unified Soil Classification System). ASTM International, West Conshohocken, PA.
- Benamar, A., dos Santos, R.N.C., Bennabi, A., and Karoui, T. 2019. Suffusion evaluation of coarse-graded soils from Rhine dikes. *Acta Geotechnica*, **14**(3): 815–823. doi:[10.1007/s11440-019-00782-1](https://doi.org/10.1007/s11440-019-00782-1).
- Chang, D.S., and Zhang, L.M. 2011. A stress-controlled erosion apparatus for studying internal erosion in soils. *Geotechnical Testing Journal*, **34**(6): 579–589. doi:[10.1520/GTJ103889](https://doi.org/10.1520/GTJ103889).
- Chang, D.S., and Zhang, L.M. 2013. Extended internal stability criteria for soils under seepage. *Soils and Foundations*, **53**(4): 569–583. doi:[10.1016/j.sandf.2013.06.008](https://doi.org/10.1016/j.sandf.2013.06.008).
- Cheng, K., Han, B.Y., Shao, H.L., and Xue, Z.J. 2024a. Heterogeneous characteristics of stress transmission within finer fraction of gap-graded soils and its relevance to suffusion-suffusion. *Computers and Geotechnics*, **175**: 106669. doi:[10.1016/j.compgeo.2024.106669](https://doi.org/10.1016/j.compgeo.2024.106669).
- Cheng, K., Ping, X.Y., Han, B.Y., Wu, H., and Liu, H.S. 2024b. Study on particle loss-induced deformation of gap-graded soils: role of particle stress. *Acta Geotechnica*, **19**: 7865–7892. doi:[10.1007/s11440-024-02377-x](https://doi.org/10.1007/s11440-024-02377-x).
- Cheng, K., Wang, Y., and Yang, Q. 2018. Semi-resolved CFD-DEM model for seepage-induced fine particle migration in gap-graded soils. *Computers and Geotechnics*, **100**: 30–51. doi:[10.1016/j.compgeo.2018.04.004](https://doi.org/10.1016/j.compgeo.2018.04.004).
- Choe, Y., Choi, H., and Won, J. 2024. Suffusion of a sand-clay mixture: impact of the ionic-concentration gradient, clay type, sand-grain size and hydraulic gradient. *Géotechnique*, **74**(10): 1004–1018. doi:[10.1680/jgeot.21.00335](https://doi.org/10.1680/jgeot.21.00335).
- Clark, P.J., and Evans, F.C. 1954. Distance to nearest neighbor as a measure of spatial relationships in populations. *Ecology*, **35**: 445–453. doi:[10.2307/1931034](https://doi.org/10.2307/1931034).
- Cui, Y.F., Zhou, X.J., and Guo, C.X. 2017. Experimental study on the moving characteristics of fine grains in wide grading unconsolidated soil under heavy rainfall. *Journal of Mountain Science*, **14**(3): 417–431. doi:[10.1007/s11629-016-4303-x](https://doi.org/10.1007/s11629-016-4303-x).
- Deng, Z.Z., and Wang, G. 2022. A 3D visualization method for identifying fabric characteristics during suffusion using transparent soil. *Canadian Geotechnical Journal*, **59**(10): 1833–1843. doi:[10.1139/cgj-2021-0191](https://doi.org/10.1139/cgj-2021-0191).
- Horikoshi, K., and Takahashi, A. 2015. Suffusion-induced change in spatial distribution of fine fractions in embankment subjected to seepage flow. *Soils and Foundations*, **2**(49): 1708–1713.
- Hunter, R.P., and Bowman, E.T. 2018. Visualization of seepage-induced suffusion and suffusion within internally erodible granular media. *Géotechnique*, **68**(10): 918–930. doi:[10.1680/jgeot.17.P.161](https://doi.org/10.1680/jgeot.17.P.161).
- Indraratna, B., Haq, S., Rujikiatkamjorn, C., and Israr, J. 2022. Microscale boundaries of internally stable and unstable soils. *Acta Geotechnica*, **17**(5): 2037–2046. doi:[10.1007/s11440-021-01321-7](https://doi.org/10.1007/s11440-021-01321-7).



- Indraratna, B., Israr, J., and Li, M. 2018. Inception of geohydraulic failures in granular soils—an experimental and theoretical treatment. *Géotechnique*, **68**(3): 233–248. doi:[10.1680/jgeot.16.P.227](https://doi.org/10.1680/jgeot.16.P.227).
- Indraratna, B., Israr, J., and Rujikiatkamjorn, C. 2015. Geometrical method for evaluating the internal instability of granular filters based on constriction size distribution. *Journal of Geotechnical and Geoenvironmental Engineering*, **141**(10): 04015045. doi:[10.1061/\(ASCE\)GT.1943-5606.0001343](https://doi.org/10.1061/(ASCE)GT.1943-5606.0001343).
- Johnston, I., Murphy, W., and Holden, J. 2021. A review of floodwater impacts on the stability of transportation embankments. *Earth-Science Reviews*, **215**: 103553. doi:[10.1016/j.earscirev.2021.103553](https://doi.org/10.1016/j.earscirev.2021.103553).
- Johnston, I., Murphy, W., and Holden, J. 2023. Alteration of soil structure following seepage-induced internal erosion in model infrastructure embankments. *Transportation Geotechnics*, **42**: 101111. doi:[10.1016/j.trgeo.2023.101111](https://doi.org/10.1016/j.trgeo.2023.101111).
- Ke, L., and Takahashi, A. 2012. Strength reduction of cohesionless soil due to internal erosion induced by one-dimensional upward seepage flow. *Soils and Foundations*, **52**(4): 698–711. doi:[10.1016/j.sandf.2012.07.010](https://doi.org/10.1016/j.sandf.2012.07.010).
- Ke, L., and Takahashi, A. 2014. Experimental investigations on suffusion characteristics and its mechanical consequences on saturated cohesionless soil. *Soils and Foundations*, **54**(4): 713–730. doi:[10.1016/j.sandf.2014.06.024](https://doi.org/10.1016/j.sandf.2014.06.024).
- Kenney, T., and Lau, D. 1985. Internal stability of granular filters. *Canadian Geotechnical Journal*, **22**(2): 215–225. doi:[10.1139/t85-029](https://doi.org/10.1139/t85-029).
- Kuo, C.Y., and Freeman, R.B. 2000. Imaging indices for quantification of shape, angularity, and surface texture of aggregates. *Transportation Research Record: Journal of the Transportation Research Board*, **1721**(1): 57–65. doi:[10.3141/1721-07](https://doi.org/10.3141/1721-07).
- Lade, P.V., Liggio, C.D., Jr., and Yamamuro, J.A. 1998. Effects of non-plastic fines on minimum and maximum void ratios of sand. *Geotechnical Testing Journal*, **21**(4): 336–347. doi:[10.1520/GTJ11373J](https://doi.org/10.1520/GTJ11373J).
- Lei, X., Yang, Z., He, S., Liu, E., Wong, H., and Li, X. 2017. Numerical investigation of rainfall-induced fines migration and its influences on slope stability. *Acta Geotechnica*, **12**(6): 1431–1446. doi:[10.1007/s11440-017-0600-y](https://doi.org/10.1007/s11440-017-0600-y).
- Locke, M., Indraratna, B., and Adikari, G. 2001. Time-dependent particle transport through granular filters. *Journal of Geotechnical and Geoenvironmental Engineering*, **127**(6): 521–529. doi:[10.1061/\(ASCE\)1090-0241\(2001\)127:6\(521\)](https://doi.org/10.1061/(ASCE)1090-0241(2001)127:6(521)).
- Luo, Y., Nie, M., and Xiao, M. 2017. Flume-scale experiments on suffusion at bottom of cutoff wall in sandy gravel alluvium. *Canadian Geotechnical Journal*, **54**(12): 1716–1727. doi:[10.1139/cgj-2016-0248](https://doi.org/10.1139/cgj-2016-0248).
- Ma, G.D., Bui, H.H., Lian, Y.J., Tran, K.M., and Nguyen, G.D. 2022. A five-phase approach, SPH framework and applications for predictions of seepage-induced internal erosion and failure in unsaturated/saturated porous media. *Computer Methods in Applied Mechanics and Engineering*, **401**: 115614. doi:[10.1016/j.cma.2022.115614](https://doi.org/10.1016/j.cma.2022.115614).
- Marot, D., Rochim, A., Nguyen, H.H., Bendahmane, F., and Sibille, L. 2016. Assessing the susceptibility of gap-graded soils to internal erosion: proposition of a new experimental methodology. *Natural Hazards*, **83**(1): 365–388. doi:[10.1007/s11069-016-2319-8](https://doi.org/10.1007/s11069-016-2319-8).
- Mehdizadeh, A., Disfani, M.M., and Shire, T. 2021. Post-erosion mechanical response of internally unstable soil of varying size and flow regime. *Canadian Geotechnical Journal*, **58**: 531–539. doi:[10.1139/cgj-2019-0790](https://doi.org/10.1139/cgj-2019-0790).
- Moffat, R., Fannin, R.J., and Garner, S.J. 2011. Spatial and temporal progression of internal erosion in cohesionless soil. *Canadian Geotechnical Journal*, **48**(3): 399–412. doi:[10.1139/T10-071](https://doi.org/10.1139/T10-071).
- Mousavi, M., Disfani, M.M., Black, J.R., and Mehdizadeh, A. 2025. Impact of sample preparation on erosion characteristics and subsequent mechanical behaviour of gap-graded soils: an imaging-based analysis. *Canadian Geotechnical Journal*, **62**: 1–19. doi:[10.1139/cgj-2024-0759](https://doi.org/10.1139/cgj-2024-0759).
- Mu, L.L., Zhang, P.Y., Shi, Z.H., and Huang, M.S. 2023. Coupled CFD–DEM investigation of erosion accompanied by clogging mechanism under different hydraulic gradients. *Computers and Geotechnics*, **153**: 105058. doi:[10.1016/j.compgeo.2022.105058](https://doi.org/10.1016/j.compgeo.2022.105058).
- Nguyen, C.D., Benahmed, N., Andò, E., Sibille, L., and Philippe, P. 2019. Experimental investigation of microstructural changes in soils eroded by suffusion using X-ray tomography. *Acta Geotechnica*, **14**(3): 749–765. doi:[10.1007/s11440-019-00787-w](https://doi.org/10.1007/s11440-019-00787-w).
- Prasomsri, J., and Takahashi, A. 2021. Experimental study on suffusion under multiple seepages and its impact on undrained mechanical responses of gap-graded soil. *Soils and Foundations*, **61**(6): 1660–1680. doi:[10.1016/j.sandf.2021.10.003](https://doi.org/10.1016/j.sandf.2021.10.003).
- Raut, A.K., and Indraratna, B. 2008. Further advancement in filtration criteria through constriction-based technique. *Journal of Geotechnical and Geoenvironmental Engineering*, **134**(6): 883–887. doi:[10.1061/\(ASCE\)1090-0241\(2008\)134:6\(883\)](https://doi.org/10.1061/(ASCE)1090-0241(2008)134:6(883)).
- Rochim, A., Marot, D., Sibille, L., and Le, V.T. 2017. Effects of hydraulic loading history on suffusion susceptibility of cohesionless soils. *Journal of Geotechnical and Geoenvironmental Engineering*, **143**(7): 1–10. doi:[10.1061/\(ASCE\)GT.1943-5606.0001673](https://doi.org/10.1061/(ASCE)GT.1943-5606.0001673).
- Shire, T., and O’Sullivan, C. 2016. Constriction size distributions of granular filters: a numerical study. *Géotechnique*, **66**(10): 826–839. doi:[10.1680/jgeot.15.P.215](https://doi.org/10.1680/jgeot.15.P.215).
- Sibille, L., Marot, D., and Sail, Y. 2015. A description of internal erosion by suffusion and induced settlements on cohesionless granular matter. *Acta Geotechnica*, **10**(6): 735–748. doi:[10.1007/s11440-015-0388-6](https://doi.org/10.1007/s11440-015-0388-6).
- Wan, C.F., and Fell, R. 2008. Assessing the potential of internal instability and suffusion in embankment dams and their foundations. *Journal of Geotechnical and Geoenvironmental Engineering*, **134**(3): 401–407. doi:[10.1061/\(ASCE\)1090-0241\(2008\)134:3\(401\)](https://doi.org/10.1061/(ASCE)1090-0241(2008)134:3(401)).
- Xia, Z., Wang, J., Zhu, Z., Hu, W., Tracy, S., and Zhao, B. 2024. Progressive internal erosion during triaxial shearing: an X-ray micro-computed tomography study. *Géotechnique*. In press. doi:[10.1680/jgeot.23.00107](https://doi.org/10.1680/jgeot.23.00107).
- Yang, J., Yin, Z.Y., Laouafa, F., and Hicher, P.Y. 2019. Modeling coupled erosion and filtration of fine particles in granular media. *Acta Geotechnica*, **14**(6): 1615–1627. doi:[10.1007/s11440-019-00808-8](https://doi.org/10.1007/s11440-019-00808-8).